



# Borehole geophysical techniques to define stratigraphy, alteration and aquifers in basalt

Catherine M. Helm-Clark<sup>a,b,\*</sup>, David W. Rodgers<sup>a</sup>, Richard P. Smith<sup>b</sup>

<sup>a</sup>Department of Geosciences, Idaho State University, Pocatello, ID 83209-8072, USA

<sup>b</sup>Idaho National Engineering and Environmental Laboratory, P.O. Box 1625, Mail Stop 2107, Idaho Falls, ID 83415, USA

Accepted 26 June 2003

## Abstract

This paper concerns the interpretation of borehole geophysical data from basalt sequences, especially continental basalt sequences that host aquifers. Based on modifications of the rules used for interpreting borehole data from sedimentary rocks, new rules are proposed to identify the internal stratigraphy, aquifer boundaries, and alteration features in continental basalts.

The value of several wireline tools is critiqued. Natural gamma logs have limited utility in basalt sequences unless anomalously high-potassium or low-potassium basalt flows and/or sedimentary interbeds exist which can act as marker beds for stratigraphic correlations. Neutron logs can usually discriminate between individual flows, flow breaks and interbeds, even in unsaturated basalts. Neutron logs and temperature logs can also be used to map aquifer thickness in basalt. Gamma–gamma density logs are usually sensitive to the density contrasts between interbeds and basalt flows, and in combination with neutron and natural gamma logs are crucial for the correct interpretation of large void spaces in basalt such as collapsed lava tubes and formerly inflated pahoehoe lobes. Basalt porosity calculated from neutron, resistivity and/or gamma–gamma density logs is commonly overestimated due to the presence of hydrous alteration minerals. Velocity and resistivity logs are best at discriminating between flows in saturated conditions. Magnetic susceptibility logs may capture magnetic mineralogy variations at a finer scale than that of flows and flow breaks and therefore should always be interpreted in combination with other logs. Non-spectral neutron–gamma logs are not useful in basalt, though spectral neutron–gamma logs have been used successfully for stratigraphic correlation and to locate pollutants.

Geochemical logs or the inclination of magnetic remanence provides the best data to discriminate individual flows with a basalt sequence, and thus establish an internal stratigraphy. Other tools used alone cannot provide reliable stratigraphic information, but a combination of tools may work. We recommend the combination of natural gamma, neutron, and gamma–gamma density logs in unsaturated rocks, and these logs plus velocity and resistivity logs in saturated rocks.

© 2003 Published by Elsevier B.V.

**Keywords:** Borehole geophysics; Basalt aquifers

## 1. Introduction

Basalt stratigraphy has become an important issue in recent years because basalt sequences can host large aquifers. Extracting adequate water for con-

\* Corresponding author. Currently at: Idaho National Engineering and Environmental Laboratory, P.O. Box 1625, Mail Stop 2107, Idaho Falls, ID 83415, USA. Tel.: +1-208-526-4314; fax: +1-208-526-0875.

E-mail addresses: [helmccath@isu.edu](mailto:helmccath@isu.edu), [helmcc@inel.gov](mailto:helmcc@inel.gov) (C.M. Helm-Clark), [rodgdavi@isu.edu](mailto:rodgdavi@isu.edu) (D.W. Rodgers), [rps3@inel.gov](mailto:rps3@inel.gov) (R.P. Smith).

sumption and agriculture while protecting the aquifer from pollution requires a thorough understanding of basalt architecture. Accordingly, this paper reviews the utility of borehole geophysical tools in determining stratigraphic features of continental basalts. Much of this knowledge, the result of the abundant wireline data generated by the Deep Sea Drilling Program (DSDP), its successor, the Ocean Drilling Program (ODP) and the International Continental Drilling Program (ICDP), is relatively new or unknown outside of the marine geophysics community. Little of this data has crossed into other disciplines like geological engineering and hydrogeology, and a comprehensive interdisciplinary review of developments in wireline logging in basalt is clearly needed.

Wireline logging to establish basalt stratigraphy is usually difficult. The composition and texture of most basalts are rather uniform and many conventional geological and geophysical tools cannot discriminate their variation. This is especially true in continental flood basalts where thin but laterally extensive flows commonly display a uniformity of physical properties measured by conventional wireline tools (Crosby and Anderson, 1971). Furthermore, wireline responses in basalt can vary greatly depending on whether logging conditions are saturated or unsaturated. Most borehole geophysical surveys in basalt have been conducted where the basalt was saturated with drilling mud, saltwater, or fresh water. This has been the case for all oceanic basalts (Goldberg, 1997; Becker et al., 1989) and for many continental flood basalts like the Deccan Traps in India which host shallow unconfined aquifers (Buckley and Oliver, 1990; Versey and Singh, 1982; C. Cheney, pers. comm.). There are few wireline studies in unsaturated basalts (Crosby and Anderson, 1971; cf. Last and Horton, 2002). One exception is the geophysical logging program at the Idaho National Engineering and Environmental Laboratory (INEEL), which has generated perhaps the largest collection of wireline logs for continental basalts in both saturated and unsaturated conditions. We have mined the INEEL Hydrogeological Data Repository (HDR) extensively for examples used in this paper.

This paper will demonstrate the value and the pitfalls of wireline logging in continental basalt. The data and results are derived from published investigations of basalt from the Deccan Traps of India, the Karoo Flood Basalts in Botswana, the island of

Hawaii, the New Jersey/Connecticut Triassic Rift Basin, the Columbia River Plateau, and the Eastern Snake River Plain. While Hawaii and similar intraplate islands are not technically continental, we include them here since the layered nature of large oceanic-island shield volcanoes closely resembles that of continental flood basalts. We begin by describing the range of continental basalt textures, and then show how different wireline tools may record these variations. The goal is to derive a valid set of interpretive rules for logging basalts in a wide variety of continental settings. Some DSDP and ODP results are also discussed to help refine on-land interpretation; to learn more about oceanic borehole geophysics in basalt, the reader is referred to the fine review papers by Goldberg (1997) and Brewer et al. (1998).

## 2. Basalt types and morphologies

A basalt can be classified by its composition, texture, and magnetic character and distinguished from other basalts by variations in these properties. Compositional and magnetic variations are described in later sections but textural properties such as flow thickness, fracture patterns, and the nature of vertical sequences are so important to wireline interpretation that they are described in more detail here.

The most common morphologic type of basalt is pahoehoe lava (Ehlers and Blatt, 1982; Macdonald, 1972). Pahoehoe flows are typically vesicular and fractured at their top and bottom boundaries, but massive in their centers. Flow tops and bottoms can be cindery or scoriaceous. The top of a pahoehoe flow commonly forms a solid ropey rind under which magma can travel great distances, either as sheet flow or through lava tubes. Flow bottoms are commonly oxidized and flow tops may be glassy. In contrast, the interiors of flows cool more slowly than the margins, resulting in larger grain sizes, little to no vesicles, and few to no fractures.

Pahoehoe flows can vary from less than 3 m to as much as 50 m thick, regardless of horizontal extent. Typically, an erupting flow will form a hummocky surface whose undulations can have amplitudes from 1 to 15 m. The lateral extent of pahoehoe is highly variable, with some flows extending less than 1 km from their vents, like those on the Snake River Plain

130 (Hughes et al., 1999); others extending tens of kilo-  
 131 meters, like on Hawaii (Stolper et al., 1996); and some  
 132 extending for over 500 km, like the basalt flows of the  
 133 Deccan Traps (Versey and Singh, 1982).

134 Pahoehoe can erupt from the vents of shield  
 135 volcanoes or from fissures. Close to a vent, scoria,  
 136 cinders, and very thinly bedded (<2 m) shelly pahoehoe  
 137 are not uncommon (e.g., Greeley and King, 1975;  
 138 Sharp, 1976). Along the leading edge of an erupting  
 139 flow, lobes of pahoehoe become inflated with magma  
 140 which can break out to form more hummocky lobes,  
 141 thus expanding the flow area (e.g., Hughes et al.,  
 142 1999). Between the eruptive vent or fissure and the

143 advancing flow front, basaltic magma typically travels  
 144 through conduits such as lava tubes and inflated lobes  
 145 (Greeley, 1982a; Macdonald, 1972). These conduit  
 146 features will eventually collapse, creating cavity-rich  
 147 basalt rubble. Substantial talus and sedimentary ma-  
 148 terial can accumulate in these feature both before and  
 149 after collapse (Greeley, 1982b).

150 In contrast to pahoehoe flows, the less-common aa  
 151 flows are characterized by rubbly flow fronts and  
 152 rubbly-to-blocky flow tops (Ehlers and Blatt, 1982).  
 153 Typically, aa is less vesicular than pahoehoe and is  
 154 laterally limited. Some pahoehoes grade into aa at  
 155 their flow fronts as a result of degassing and increased

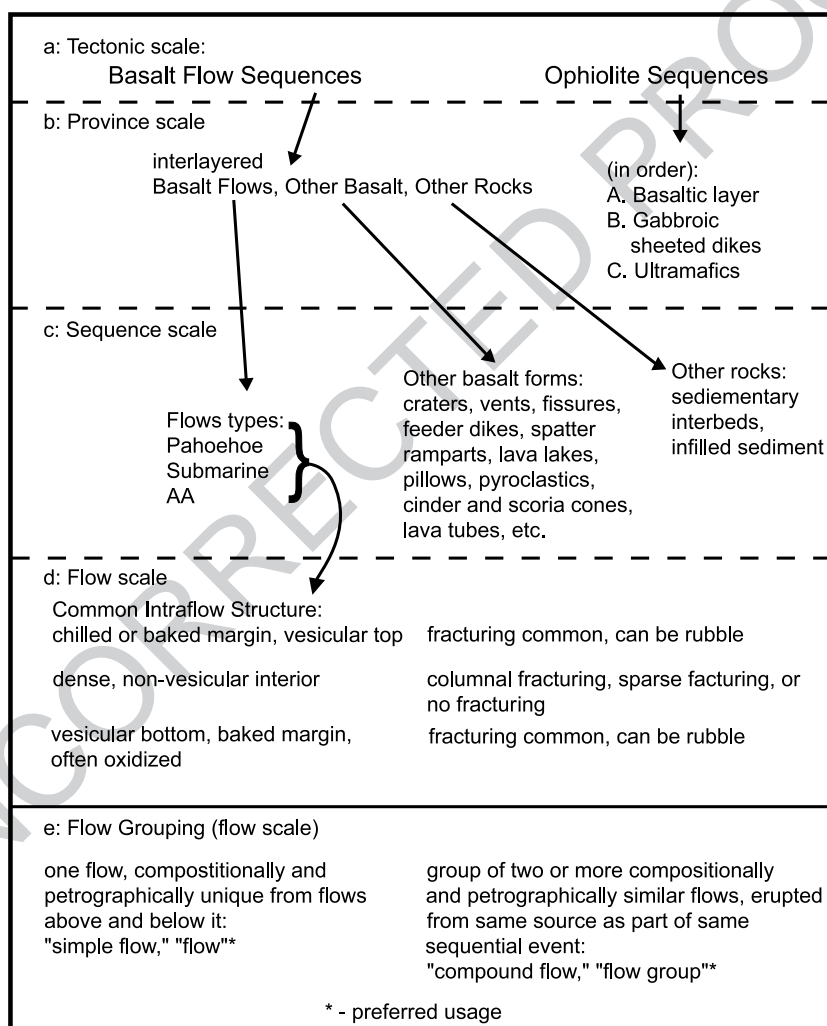


Fig. 1. A simplified hierarchy of basalt features at several scales.

viscosity from cooling. Other aa flows erupt directly, as they do on Iceland (Macdonald, 1972).

Most pillow basalts form on the ocean floor (Anderson et al., 1982) but rarely in continental basalt flow sequences. Because of their comparative rarity on land, we do not discuss pillow basalts in this study, but refer the reader to the work of Haggas et al. (2002), Brewer et al. (1998), and Brewer et al. (1990), as well as to the copious literature of the DSDP and ODP.

In all basalts, cracks and fractures become the sites of secondary mineral growth. Alteration typically starts near flow margins and works inward (Cheney, 1981). Common secondary minerals include calcite, clays, and/or zeolites. Vesicles are also sites of secondary mineral growth and alteration, like the abundant amygdales of the Deccan Traps (Buckley and

Oliver, 1990). Younger basalts are more likely to host unaltered and unfilled vesicles than older ones. For all basalt flows, post-emplacement erosion and soil development can both destroy flow surfaces and cause rubble formation at the tops of flows. Depending on the time elapsed between basalt eruptions, a sedimentary interbed or “intertrappean” layer may develop and be preserved in the geologic record. Examples include beach sediments as interbeds on Hawaii (Beeson et al., 1996), and loess sediment interbeds on the windswept East Snake River Plain (Hughes et al., 1999; Blair, 2002).

Most basalt occurs not as individual layers but as thick sequences of lava flows with sedimentary interbeds. Flows can be either simple or complex (Walker, 1972) (see Fig. 1). Simple flows are compositionally

t1.1 Table 1

t1.2 Tectonic classification of basalt

t1.3	Tectonics	Size	Composition	Principal minerals	Common morphological features	Examples
t1.4	<i>Oceanic spreading centers and ocean floor</i>					
t1.5	Divergent boundary between two oceanic plates	70% of the Earth's surface	Mid-Ocean Ridge Basalts (MORB), mostly olivine tholeiites, low K, low Ti; often pervasively serpentinized	Olivine, calcium-rich plagioclase	Ophiolites: pillow basalts, shallow dikes and sills, gabbroic sheeted dikes, basal ultramafics	East Pacific Rise, California Coast Range Ophiolite
t1.6	<i>Oceanic island chains and plateaus</i>					
t1.7	Intraplate, thought to be fed by mantle plume	Variable	Ocean Island Basalts (OIB): tholeiite and occasional late alkali basalt; enriched in K, Th and U with respect to MORB	Tholeiite: calcium-rich plagioclase, pyroxene, commonly olivine alkali: olivine, feldspathoids	Large shield volcanoes, hyaloclastites, pillow basalt, linear rifts and fissures, lava tubes, compound flows of pahoehoe and aa	Hawaii, Reunion
t1.9	<i>Continental flood basalts</i>					
t1.10	Intraplate, extensional regime, continental rift or mantle plume	>100,000 km <sup>3</sup> (“flood basalt”)	Continental Flood Basalts (CFB): tholeiites, andesitic basalts, typically richer in Si and K than MORB	Clinopyroxene, plagioclase	Mostly laterally extensive pahoehoe sheets, compound flows close to vents, simple flows distally; pillow and palagonite complexes	Karoo Flood Basalts, Deccan Traps, Columbia River Plateau
t1.11	<i>Continental volcanic fields</i>					
t1.12	Intraplate, extensional regimes; (“plains basalts”; basin and range volcanism)	<100,000 km <sup>3</sup>	A large variety of basaltic and andesitic rocks, often associated with bimodal volcanism	Clinopyroxene, plagioclase, and/or olivine; feldspathoids in alkali basalts	Small low-angle shields, lava tubes and vents feeding surface flows; laterally limited, simple and compound flows; small cinder and scoria cones	East Snake River Plain (ESRP), Clear Lake Volcanic Field

188 unrelated to the flows immediately above and below  
 189 them. They have a discernable top, middle, and  
 190 bottom, and their geochemistry and petrography are  
 191 distinct. Compound flows are clusters of flow units all  
 192 sharing the same geochemical and petrographic fea-  
 193 tures. This uniformity of physical properties suggests  
 194 strongly they were erupted from the same source in a  
 195 short period of time. The flow units in a compound  
 196 flow usually have a preserved flow top to distinguish  
 197 them from other flow units. There should be little to  
 198 no soil or sediment separating each flow unit. In some  
 199 basalt provinces, e.g., the Deccan Traps, a flow may  
 200 be compound near its vent and a simple flow at  
 201 distance (Versey and Singh, 1982). When using wire-  
 202 line tools in a borehole, it may be impossible to  
 203 determine if a flow is a simple flow or an individual  
 204 flow unit of a compound flow, depending on the  
 205 choice of wireline tools used. For this reason, some  
 206 researchers prefer to use the terms flow groups and  
 207 flows instead of compound flows and flow units (e.g.,  
 208 Kuntz et al., 1980; Anderson and Lewis, 1989). For  
 209 convenience, this is the usage we prefer and will use  
 210 for the remainder of this paper.

211 Different basalt compositions occur in different  
 212 tectonic environments, and those environments com-  
 213 monly exert a controlling influence on the morphol-  
 214 ogy of basalt. It is useful exercise, therefore, to  
 215 classify basalt by tectonic environment (see Table  
 216 1). If we know how tectonic environment influences  
 217 basalt, then we will have a preliminary idea of what to  
 218 expect during drilling and wireline logging. For ex-  
 219 ample, geothermal exploration near The Geysers geo-  
 220 thermal field might encounter the pillow basalts of the  
 221 California Coast Range ophiolite (Bailey et al., 1964).  
 222 In comparison, ground water investigations on the  
 223 Columbia River Plateau will likely encounter the 500-  
 224 km-long, ~ 50-m-thick Grande Ronde flow of the  
 225 Columbia River flood basalts (Hooper, 1997).

### 226 3. Wireline logging of basalt

227 Having outlined the common features of basalt  
 228 morphology which can be used to describe the stra-  
 229 tigraphy of a basalt flow sequence, we need to  
 230 examine the wireline tools which can measure these  
 231 and other stratigraphic features. We classify strati-  
 232 graphic features as either primary or secondary. Pri-

mary features are those intrinsic to the basalt itself, 233  
 such as composition or vesicularity. Secondary fea- 234  
 tures are not intrinsic; however, they are related in 235  
 some way to basalt and are useful in establishing 236  
 stratigraphy, e.g., the presence of interbeds or saturat- 237  
 ed vs. unsaturated conditions. 238

In the description of wireline tools which follows, 239  
 we describe the basis of each tool, its application to 240  
 basalt, and potential problems of interpretation in 241  
 basalt. Not all logs are discussed. Some, like the 242  
 caliper log, are so straightforward that discussion is 243  
 deemed unnecessary. Other logs, like flowmeters, 244  
 behave the same regardless of the rock type. Some 245  
 tools like nuclear magnetic resonance are relatively 246  
 new and have little to no track record yet in basalt. 247  
 Some tools are so specialized that they have little 248  
 application to basalt. Much of the discussion concerns 249  
 tool categories, not specific tools. For example, resis- 250  
 tivity is one of several tool categories, whereas 251  
 laterologs, point resistance, and induction tools are 252  
 specific tools in that category. 253

### 4. Natural gamma logs 254

Three naturally occurring radioisotopes have decay 255  
 chains and modes involving the emission of gamma 256  
 rays, specifically  $^{40}\text{K}$ ;  $^{238}\text{U}$  and its daughter products; 257  
 plus  $^{232}\text{Th}$  and its daughter products. The energy 258  
 spectrum of these decays is concentrated between 259  
 0.2 and 3.0 MeV. A natural gamma log records total 260  
 decay events across the gamma energy spectrum. 261  
 Most modern natural gamma results are reported in 262  
 API units (Belknap et al., 1960; Keys, 1990). A 263  
 variation of the natural gamma log is the spectral 264  
 gamma log, which discriminates the contribution of 265  
 different parts of the gamma energy spectrum 266  
 (Schlumberger Wireline and Testing, 1989). Since 267  
 K, Th, and U contribute to different parts of the 268  
 gamma energy spectrum, this information can be used 269  
 to determine the concentration of each of these ele- 270  
 ments, respectively. 271

### 5. Natural gamma logs—basalt applications 272

The natural gamma log is sensitive to several 273  
 stratigraphic characteristics in basalt, the most impor- 274

275 tant of which is anomalous potassium content in  
 276 basalt and clayey interbeds. Basalts have very low  
 277 potassium, uranium, and thorium concentrations,  
 278 where potassium content usually dominates the natural  
 279 gamma signature (e.g., Hughes et al., 2002;  
 280 Anderson and Bartholomay, 1995; Versey and Singh,  
 281 1982). Natural gamma counts for a basalt are typically  
 282 between 5 and 50 API.

283 Variable potassium content can sometimes be used  
 284 as a primary stratigraphic feature in basalt. The  
 285 composition of basalt is commonly uniform within a  
 286 basalt province and there is little variation in K  
 287 concentration, e.g., the Karoo flood basalt remnant  
 288 exposed in Botswana (Cheney, 1981; Cheney and  
 289 Farr, 1980). In other basalt provinces, however,  
 290 anomalously high or low K-content basalt flows exist  
 291 in the subsurface, and these flows can be used as  
 292 marker beds for establishing stratigraphic correlations,  
 293 e.g., the Deccan Traps (Buckley and Oliver, 1990).

294 An important secondary stratigraphic feature is the  
 295 clay content of sedimentary interbeds. Sedimentary  
 296 interbeds commonly contain higher levels of potassi-  
 297 um, uranium, and/or thorium than the flows them-  
 298 selves. This is mainly due to lithological differences,  
 299 most notably the presence of clays and other phyllo-

300 silicates minerals which have intrinsically higher  
 301 radioisotope content than basalt (Buckley and Oliver,  
 302 1990).

## 6. Natural gamma logs—results and interpretations 303

304 Natural gamma logs may be used for correlating  
 305 basalt flows between boreholes if high-gamma emit-  
 306 ting interbeds and/or anomalously high- or low-  
 307 gamma emitting basalt flows are present. Fig. 2 is  
 308 a cross section through the Deccan Traps in the  
 309 Betwa Basin in central India, showing an anom-  
 310 alously high gamma-emitting basalt with respect to its  
 311 neighbors (labeled A on Fig. 2). Evidence from  
 312 lithological logs and geochemical analyses of sub-  
 313 surface samples demonstrates that a handful of  
 314 Betwa Basin flows are consistently higher in natural  
 315 gamma emissions when compared to most other  
 316 flows (Versey and Singh, 1982). These higher-pot-  
 317 asium flows do not show lateral variation in their total  
 318 natural gamma measurements, even when traced over  
 319 tens of kilometers. Using geochemical measure-  
 320 ments, Versey and Singh (1982) determined that  
 321 the high-gamma flows had ~ 4 times the K<sub>2</sub>O and

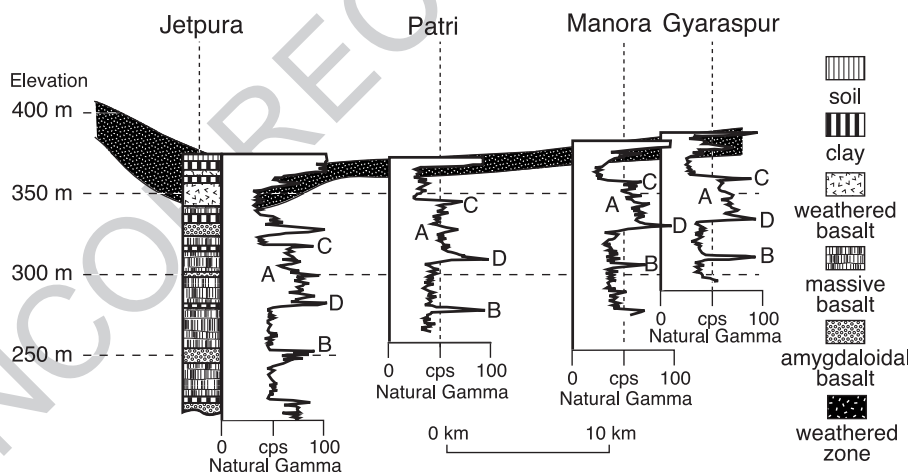


Fig. 2. The natural gamma logs shown here are for boreholes in the Deccan Trap flood basalts in central India. Log data was collected in saturated conditions. Natural gamma counts increase to the right in this figure. Geology and log interpretations are based on Versey and Singh (1982) and Buckley and Oliver (1990), who used lithological logs and geochemical analyses to define their stratigraphy. The ~ 50-m-thick high-natural-gamma-count basalt is a marker bed (labeled A) which can be traced over 50 km. The narrow spike (labeled B) below the 50-m-thick basalt is not an interbed, but an altered amygdaloidal basalt flow. The “horns” labeled C and D at the top and bottom of the high-natural-gamma basalt layer A correspond to clay beds. This figure is modified from Buckley and Oliver (1990).

322 2 to 3 times the Th content compared to the majority  
 323 of other local flows, thus demonstrating that the  
 324 increased gamma emissions are due to differences  
 325 in the basalts themselves, and not due to the pres-  
 326 ence of amygdales or secondary alteration minerals.  
 327 These characteristics make it possible to use this and  
 328 similar high-gamma flows as marker beds, enabling  
 329 correlations of flows over distances as great as 100  
 330 km (Buckley and Oliver, 1990; Versey and Singh,  
 331 1982).

332 Fig. 3 shows a cross section through the Eastern  
 333 Snake River Plain. The logs shown here were  
 334 collected over a 50-year period using a variety of  
 335 wireline tools, so the results are relative and qual-  
 336 itative only. Even so, the interpretation of these logs

337 is based on comparison with the continuously col-  
 338 lected cores from three deep boreholes along or near  
 339 this cross section. Several features on the logs can  
 340 be therefore correlated between wells with confi-  
 341 dence. In Fig. 3, the high-gamma count interbed  
 342 labeled “A” pinches out to the north as it gains in  
 343 elevation, a behavior observed in present-day loess  
 344 deposited on the sides of volcanic cones at nearby  
 345 Craters of the Moon National Monument. Feature B  
 346 is the flow boundary between a low-K flow group  
 347 above and a higher-K flow group below, making this  
 348 feature a usable stratigraphic marker. Feature C in  
 349 Fig. 3 is a pair of interbeds. The top interbed shows  
 350 variable thickness which apparently pinches out to  
 351 the south.

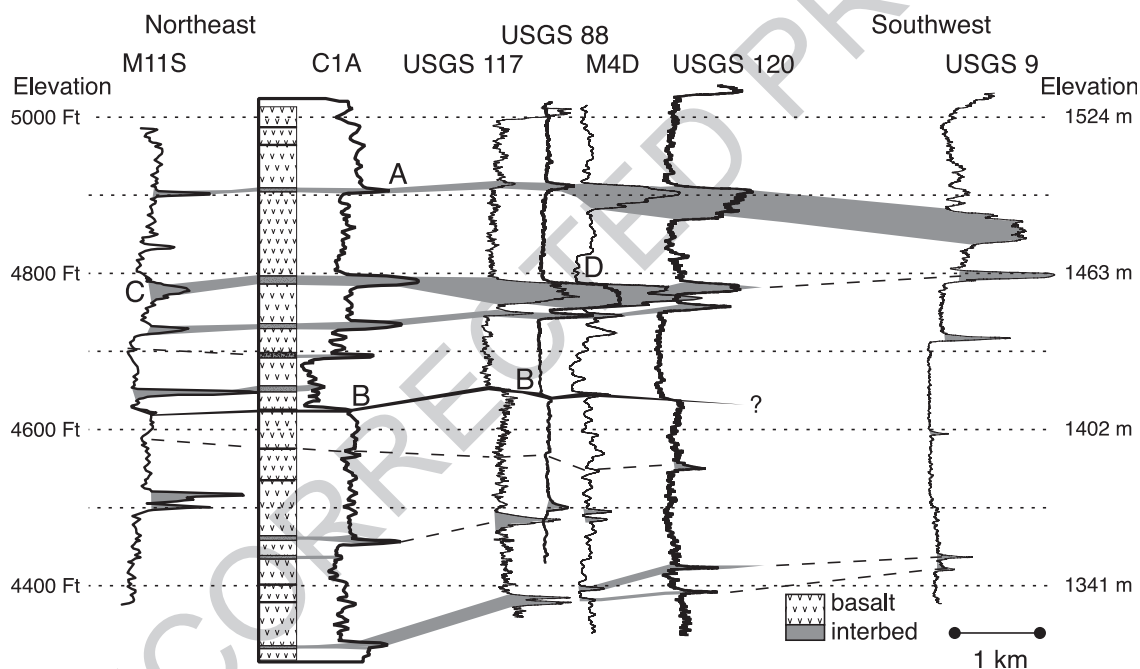


Fig. 3. Twelve-kilometer natural gamma cross section of wells on the Eastern Snake River Plain. Natural gamma counts increase to the right. The staggered vertical positions of the logs correspond to their relative elevations in the field. Logs were collected over a 50-year period using six generations of wireline tools and reporting results in three different units of measure. All log results shown here should be considered qualitative only. Interpretations are in part based on thin sections and core-to-log correlations for wells BG 77-1, USGS-118 and C1A at the Idaho National Engineering and Environmental Laboratory (INEEL) (Barraclough et al., 1976; Kuntz et al., 1980; Anderson and Lewis, 1989; Knutson et al., 1994; Anderson and Bartholomay, 1995; Blair, 2002; and unpubl. data archived at the INEEL HDR by Knutson, 1993–1994, and Helm-Clark, 2001–2002). These three wells are along or within 1 km of the cross section shown. A composite lithological log is shown here for well C1A. The stratigraphic interpretation is that of the authors. Shaded units are interbeds or flow breaks. Dotted lines are inferred flow boundaries. Features: A—high-natural-gamma-count interbed correlated in most of the wells; B—flow boundary between a low-K flow group above and a higher-K flow group below, suitable as a stratigraphic marker; C—pair of high-natural-gamma-count interbeds correlated across several wells; D—possible collapsed structure.

## 352 7. Natural gamma logs—potential problems of 353 interpretation

354 There are several factors which can lead to the  
355 misinterpretation of natural gamma logs in basalt. A  
356 common one is the lack of recognition of textural  
357 features. For example, feature D in Fig. 3 has the  
358 appearance of a low-K flow which has no correlatives  
359 in nearby wells. In fact, the wells to the north (USGS-  
360 88, USGS-117) lack this feature and the nearest well to  
361 the south (USGS-120) shows slightly elevated gamma  
362 counts at the corresponding position to feature D.  
363 Since the spacing between these wells is a kilometer  
364 or less, it is unlikely that a localized K-poor flow was  
365 erupted into such a small area. Alternatively, it is  
366 possible that the low gamma counts at D are due to a  
367 localized morphological phenomenon such as a col-  
368 lapsed lava tube, a formerly inflated pahoehoe lobe, or  
369 other void-rich feature. Pahoehoe can accommodate  
370 many void spaces. Overlying flows do not necessarily  
371 fill all the voids in flows underneath, so large voids  
372 spaces can and will occur in the subsurface (Welhan et  
373 al., 2002). Voids do not contribute any gamma decays  
374 and so will yield anomalously low natural gamma  
375 counts. Where there are no correlative low-gamma  
376 layers in nearby wells, increased void spaces should be  
377 suspected and can be confirmed by collecting a density  
378 log. Void morphology is discussed in more detail in the  
379 section on gamma–gamma density logs.

380 Interbedded sediments are not always associated  
381 with elevated gamma counts. For example, Buckley  
382 and Oliver (1990) reported a diatomite interbed in the  
383 Deccan Traps which emitted a low gamma flux and  
384 therefore had low contrast with respect to basalt. In  
385 this case, the natural gamma log could not discrimi-  
386 nate between the diatomite and basalt flows above and  
387 below it.

388 Groundwater will attenuate measured gamma  
389 counts in holes greater than  $\sim 15$  cm (6 in.), assuming  
390 that the borehole contains no drilling fluid at the time  
391 it is logged (Crosby and Anderson, 1971). The larger  
392 the hole the greater the attenuation. While this is an  
393 effect that can be seen in any type of strata, it is  
394 particularly pronounced in basalt where total gamma  
395 emissions are small and counting statistics are less  
396 favorable than in other rock types. For stratigraphic  
397 interpretation, quantitative measurement of potassium  
398 content is possible if the tool is properly calibrated

and all the necessary corrections have been made for 399  
the presence of drilling mud, water, casing, and/or 400  
borehole diameter. Without such corrections, quanti- 401  
tative correlations are impossible. Qualitative correla- 402  
tions can still be made, however, if anomalous 403  
gamma-count layers exist in the subsurface. 404

## 8. Neutron logs 405

All neutron tools employ a source of fast neutrons 406  
( $>0.1$  MeV). The effects of neutron interactions with 407  
borehole fluids, pore-space fluids, and rock matrix are 408  
subsequently measured with a variety of detectors and 409  
detector geometries. A useful parameter integral to the 410  
arrangement of detectors is the slowing-down length, 411  
 $L_s$ .  $L_s$  is the root-mean-squared distance that a fast 412  
neutron must travel before it is thermalized, i.e., before 413  
reaching the thermal energy range of  $<0.1$  eV 414  
(Schlumberger, 1989). Slowing-down length is a func- 415  
tion of the bulk density, the concentration of neutron 416  
moderators, and the scattering and capture cross sec- 417  
tions of those moderators (Broglia and Ellis, 1990). 418  
When hydrogen is present, its  $L_s$  will dominate all 419  
others due to its very large scattering and capture cross 420  
sections. For example,  $L_s$  in water is much shorter than 421  
 $L_s$  in calcite, despite the fact that calcite is the denser 422  
material. Other elements with large neutron capture 423  
cross sections like chlorine may also shorten  $L_s$ , e.g., 424  
connate brine vs. potable water. In reality, however, this 425  
effect is small and is rarely observed, even when 426  
crossing a fresh-to-saline water interface (Keys, 1990). 427

Neutron logs are usually named for what they 428  
detect. A neutron–epithermal neutron log detects 429  
neutrons in the epithermal 0.1 to 100 eV range where 430  
the detector is at a distance greater than  $L_s$  from the 431  
source. At this distance, the epithermal neutron flux 432  
will decrease as an increasing number of neutrons are 433  
thermalized. Since there are few elements that can 434  
moderate neutron flux as well as hydrogen, the flux 435  
decrease is mainly due to an increase in hydrogen 436  
content, usually with a logarithmic proportionality. A 437  
neutron–thermal neutron log operates the same way 438  
as the epithermal log, except the detector measures 439  
neutron flux in the  $<0.1$  eV range. In the thermal 440  
energy range ( $<0.1$  eV), hydrogen does not moderate 441  
thermalized neutrons, but will prefer to capture them 442  
instead. An often-used variation in neutron logging is 443

444 to place the detector at a distance less than  $L_s$  from the  
445 source. In this case, the detected epithermal or thermal  
446 neutron flux will be linearly proportional to hydrogen  
447 content. This is the basis of the moisture meter which  
448 is most often used in soils and the unsaturated zone.

449 The traditional interpretation for neutron logs in  
450 saturated rocks assumes a negative correlation be-  
451 tween water content in interconnected pore spaces  
452 and the thermal or epithermal neutron counting rate;  
453 these results can be converted into a porosity mea-  
454 surement if a material-specific calibration exists (Bro-  
455 glia and Ellis, 1990). In contrast, in unsaturated  
456 conditions, traditional neutron tools and moisture  
457 meters do not measure porosity per se, but rather are  
458 assumed to measure any moisture in the rock's pore  
459 spaces (Crosby and Anderson, 1971).

## 460 9. Neutron logs—basalt applications

461 Neutron logs can discriminate features in basalt  
462 such as flow breaks, fracture zones, alteration, inter-  
463 beds, and aquifer thickness. For example, decreased

464 neutron flux at flow breaks can help determine strati-  
465 graphic details (Crosby and Anderson, 1971; Siems,  
466 1973). Sharp decreases in neutron flux also correlate  
467 to increased fracture porosity and other permeable  
468 zones when in saturated basalt. In the unsaturated  
469 zone, flow breaks, fractures, and other permeable  
470 intervals in basalt will correspond to decreased neu-  
471 tron flux if they host increased moisture, perched  
472 ground water, or hydrous alteration minerals. Neutron  
473 logging may also distinguish secondary stratigraphic  
474 features such as sedimentary interbeds if water or  
475 hydrous minerals are present. For example, a hydro-  
476 gen-rich clay will affect the neutron flux, but an  
477 unsaturated quartz arenite will not.

## 10. Neutron logs—results and interpretations

479 Fig. 4 shows epithermal neutron logs and strati-  
480 graphic correlations from the Columbia River Plateau  
481 flood basalts (Siems, 1973). These logs are qualitative  
482 and neutron flux increases to the right. Flow groups  
483 and other strata were identified by Siems (1973) using

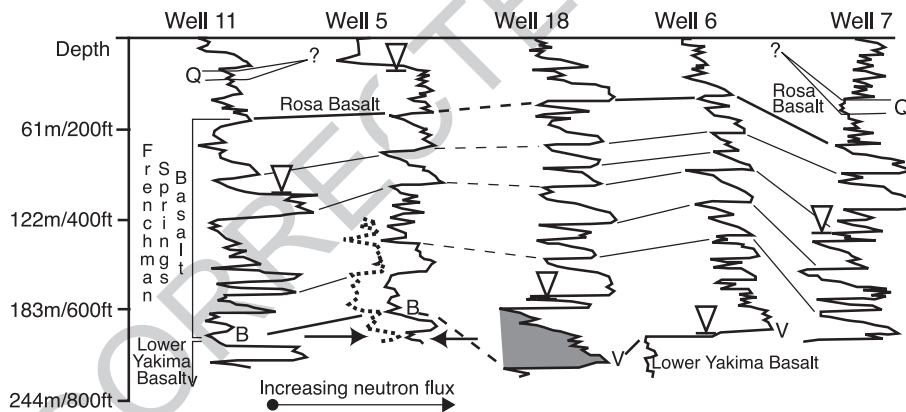


Fig. 4. Neutron cross section of wells on the Columbia River Plateau in northeast Washington State. Neutron counts increase to the right, unsaturated zone moisture/saturated porosity increases to the left. Unfortunately, all the logs from Siems (1973) were presented as qualitative data with no units of measure reported, so scale and units are not known for these logs. Black arrowheads mark the top of the unconfined aquifer. Siems (1973) recorded neutron logs at different scales above and below the water table, and spliced the data together at the water table for presentation. Black lines are correlations by Siems (1973). Dotted lines are inferred correlations. Vertical arrowheads mark the top of the water table. Feature Q is the Quincy diatomite. Feature V is the Vantage sandstone. Feature B is a blue clay/siltstone. The traverse is ~40 km long, though the spacing shown between wells is not to scale. The dotted line to the left of the neutron log for well 5 is a portion of the natural gamma log for this well. Horizontal arrows mark the location of a possible clay-rich layer, based on increased natural gamma counts plus decreased neutron counts. A known clayey layer in well 5 is the blue clay/siltstone labeled “B” just above the arrows, again where natural gamma counts increase as neutron counts decrease. The lack of the expected drop in neutron counts at the water table for wells 11 and 5 is due to the scale change in the recorded data at the water table (Siems, 1973). Wells 18, 6 and 7 do show an overall drop in average neutron counts at the water table. In wells 18 and 7, the drop is subtle, unlike well 6, where it is very abrupt. This figure is modified from Siems (1973).

484 lithological logs, petrographic and geochemical anal-  
 485 yses of cuttings, exposures of correlative flows in  
 486 nearby deeply cut river canyons, natural gamma logs,  
 487 and epithermal neutron logs. Siems (1973) identified  
 488 the Quincy diatomite (labeled “Q” on Fig. 4), the  
 489 Ventura sandstone (labeled “V”), and a variably  
 490 lithified blue clay/siltstone (labeled “B”) as interbeds

in these and several other wells in western Washing-  
 ton State. Based on lithological logs and geochemical  
 data, Siems (1973) correlated flow breaks with sharp  
 decreases in neutron flux on Fig. 4, and attributed the  
 change in flux due to increased porosity, higher water  
 content, and/or the presence of clays and other hy-  
 drous minerals.

491  
 492  
 493  
 494  
 495  
 496  
 497

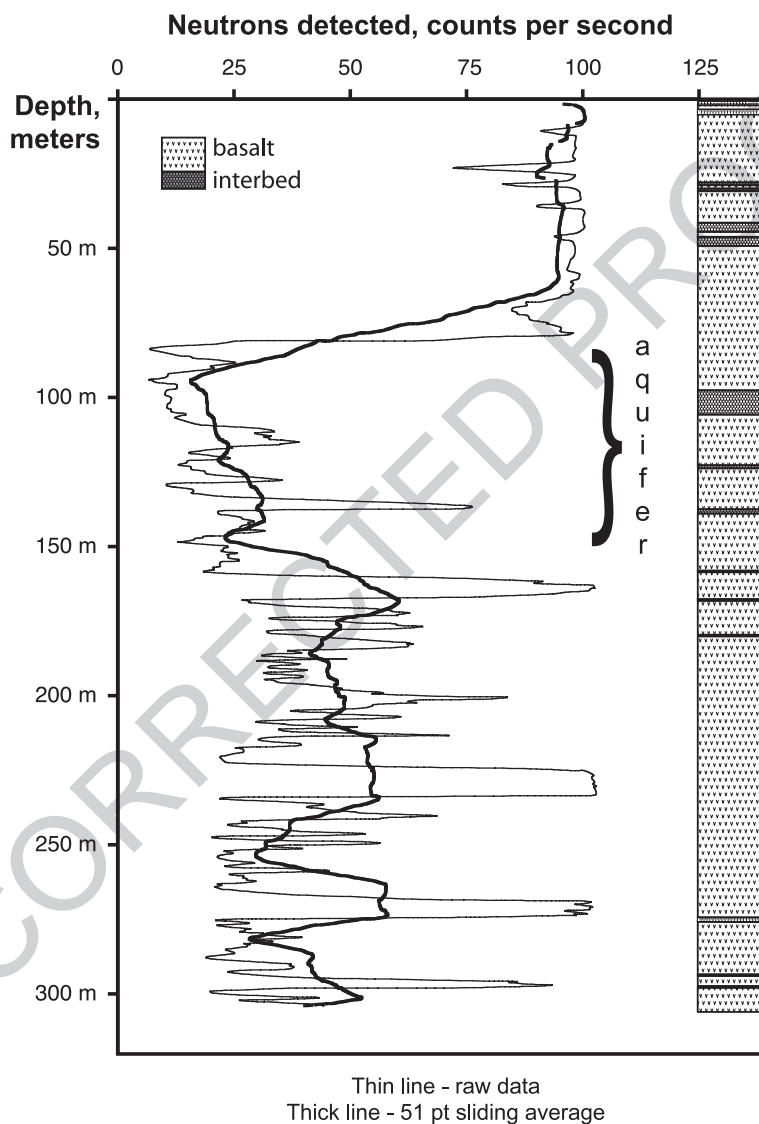


Fig. 5. Neutron counts for well USGS-30 on the Eastern Snake River Plain. Stratigraphic column from Chase et al. (1964). Thin line—neutron counting rate data. Thick line—sliding average of 51 data points to show more clearly the regions of high, low and moderate average neutron flux in the well. Unattenuated high neutron counts in unsaturated basalt are obvious above the water table. Neutron counts are lowest in the aquifer layer. Moderate neutron counts below the aquifer are interpreted as the attenuation of neutron flux by hydrous alteration minerals.

498 A portion of the natural gamma log (the dotted log  
499 trace) from well 5 is also shown in Fig. 4, next to its  
500 epithermal neutron log. The signature of hydrous  
501 minerals on this log is manifest as increasing natural  
502 gamma vs. decreasing neutron counts at two depths  
503 near the bottom of well 5. Between the arrows, the  
504 presence of hydrous minerals associated with con-  
505 verging gamma and neutron peaks is conjectural.  
506 Above the arrows, however, increasing natural gamma  
507 vs. decreasing neutron counts correlate with the blue  
508 clay/siltstone at feature B.

509 An interesting textural feature on the Columbia  
510 River Basalt logs is an overall top-to-bottom increase  
511 in the neutron flux for many flows (e.g., shaded area,  
512 well 18, Fig. 4). Siems (1973) attributed this effect to  
513 decreasing porosity from the flow top to the massive  
514 interior of each flow. Similar behavior has also been  
515 observed in saturated subsurface basalt flows on the  
516 Eastern Snake River Plain, several of which occur in  
517 INEEL boreholes including well C1A. For C1A, an  
518 increase in neutron flux is only loosely correlated with  
519 a decrease in porosity from the top to the bottom of  
520 flows (J.C. Crocker, 1992, unpubl. data archived at the  
521 INEEL HDR). C1A porosity measurements on cores,  
522 however, do not account for any fractures present in  
523 basalt flows. Based on examination of C1A cores,  
524 fractures are most prevalent at the tops of basalt flows  
525 (Helm-Clark, unpubl. data), and most of the permeable  
526 zones in the local aquifer are associated with this  
527 fracture-based porosity (Welhan et al., 2002). If the  
528 porosity measurements on core and the observed frac-  
529 ture trends of flows are both considered, then Siems's  
530 correlation of increasing neutron flux vs. decreasing  
531 porosity in saturated basalt flows appears to be true.

532 Since altered basalts can sometimes be traced over  
533 large distances in some basaltic provinces (e.g., the  
534 Deccan Traps, bed B, Fig. 2), coherent zones of  
535 alteration may be used for stratigraphic correlations.  
536 For example, using geochemical analyses of cores,  
537 Morse and McCurry (1997, 2002) showed that the  
538 bottom of the Snake River Aquifer corresponds to the  
539 top of a widespread basalt alteration zone, with  
540 authigenic minerals filling fractures, cracks, and  
541 vesicles. This alteration horizon is present in every  
542 cored well at the INEEL, spread over an area greater  
543 than 1000 km<sup>2</sup>. Such an alteration zone should be  
544 evident on INEEL epithermal neutron logs compared  
545 to unsaturated basalt, since  $L_s$  in altered basalt will be

shortened by the addition of chemically bound hydro- 546  
gen in clays and other hydrous alteration minerals. 547

548 Fig. 5 shows the epithermal neutron log for well  
549 USGS-30 at the INEEL. The top of the aquifer stands  
550 out as the steep decrease in neutron counts at ~ 80 m  
551 below land surface (bls). The bottom of the aquifer is  
552 at ~ 160 m bls, where neutron counts increase from  
553 very low average values to higher average values.  
554 These picks for the top and the bottom of the aquifer  
555 agree with the aquifer boundaries mapped by temper-  
556 ature logging in this well (Smith et al., 2002). Based on  
557 Morse and McCurry (2002), the bottom of the aquifer  
558 also corresponds to the top of the altered basalts.  
559 Compared to the unsaturated and unaltered basalts  
560 above 80 m bls, the neutron counts for the basalts  
561 below 160 m bls are moderate to low. Since the growth  
562 of authigenic minerals in fractures and other void  
563 spaces will reduce and eventually eliminate porosity,  
564 it is safe to assume that there is little free water in the  
565 subaquifer basalts. This strongly suggests that the  
566 neutron flux below the aquifer is due to the growth of  
567 hydrous alteration minerals, as Morse and McCurry  
568 (1997) suggested.

## 11. Neutron logs—potential problems of 569 interpretation 570

571 Morin et al. (1993) investigated the behavior of  
572 different source-to-detector spacings when logging in  
573 unsaturated basalt with conventional neutron logging  
574 tools. They found that for all but the widest separa-  
575 tion, their tool behaved like a moisture meter in the  
576 unsaturated zone, and not like a conventional neutron  
577 log. The spacing at which the tool began to behave  
578 like a standard neutron log (>1 m) was also far enough  
579 that the neutron flux was very low. They concluded  
580 that to prevent marginal counting statistics at large  
581 source-to-detector separation, the logging rate should  
582 be decreased or a stronger neutron source employed.  
583 The implication of this experiment is that convention-  
584 al neutron logs in unsaturated basalt should be inter-  
585 preted with caution, especially if the tool used has a  
586 source-to-detector spacing of under a meter.

587 Using neutron log results to calculate porosity in  
588 basalt is difficult. The first impediment is that most  
589 neutron tools are calibrated for sedimentary rocks.  
590 Even if a basalt-specific calibration exists, the expe- 590

591 riences of the DSDP, ODP (Broglia and Ellis, 1990),  
 592 Mt. Hood Geothermal Project (Blackwell et al., 1982),  
 593 and other logging projects in basalt (Knutson et al.,  
 594 1994) show that neutron data does not correlate  
 595 directly to interconnected porosity in basalt when  
 596 clays and/or other hydrous alteration minerals are  
 597 present. This apparent porosity excess error is not  
 598 unknown for sedimentary rocks with hydrous miner-  
 599 als and/or hydrocarbons (Schlumberger, 1989). In  
 600 general, if natural gamma and/or resistivity logs are  
 601 run in tandem with neutrons logs, these logs can help  
 602 identify basalt intervals enriched with hydrous miner-  
 603 als. Broglia and Ellis (1990) discussed at length how  
 604 to employ  $L_s$  calculations to correct neutron porosity  
 605 for alteration mineral effects in oceanic basalts. By  
 606 doing so, they were able to calculate alteration profiles  
 607 for the ODP boreholes they studied.

## 608 12. Gamma–gamma density logs

609 A gamma–gamma logging tool actively bombards  
 610 a borehole with medium-energy gamma radiation and  
 611 then measures the back-scattered and attenuated gam-  
 612 ma flux after it has reacted with the borehole envi-  
 613 ronment. The gamma–gamma log is sometimes called  
 614 an active gamma log because of the active bombard-  
 615 ment by the radioactive source in the tool. Gamma  
 616 rays with energy between 0.1 and 1 MeV interact with  
 617 orbital electrons through Compton scattering colli-  
 618 sions. Gamma rays lose some of their energy with  
 619 each Compton scattering event. This attenuation of  
 620 the active gamma flux is a function of the electron  
 621 density, and for most rocks, including basalt, electron  
 622 density is linearly proportional to bulk density. Gam-  
 623 ma rays which reach lower energies (<150 keV) are  
 624 subject to both Compton scattering and to outright  
 625 absorption. Absorption depends on the photoelectric  
 626 cross section, which is inversely related to gamma  
 627 energy and is directly related to the average atomic  
 628 number of the medium.

629 Properly calibrated and corrected gamma–gamma  
 630 logs can yield accurate and precise measurement of  
 631 bulk density in a wide range of lithologies. High  
 632 gamma flux means low density, and vice versa. The  
 633 utility and popularity of this log for density determi-  
 634 nation is the reason it is commonly referred to as a  
 635 density log or gamma–gamma density log. Photo-

electric effect as an adjunct to the gamma–gamma log 636  
 is often used in the petroleum industry to correct for 637  
 the near-field effect of mud pack in a borehole 638  
 (Schlumberger, 1989). Photoelectric effect is also used 639  
 in geochemical logging, discussed below. 640

## 13. Gamma–gamma density logs—basalt applications

641  
 642  
 643 The use of the gamma–gamma density log in basalt 643  
 is no different than in any other rock type. The 644  
 stratigraphic properties of basalt which are sensitive 645  
 to changes in bulk density are both compositional and 646  
 textural. Intraflow features are mostly textural, like 647  
 changes in vesicularity. The vesicular flow tops and 648  
 bottoms of basalt are less dense than compact and 649  
 massive flow interiors. The largest density differences, 650  
 however, are usually between flows and interbeds, the 651  
 result of both the compositional and textural changes 652  
 between basalt and most sedimentary rocks. 653

## 14. Gamma–gamma density logs—results and interpretations

654  
 655  
 656 Fig. 6 shows both the gamma–gamma density and 656  
 epithermal neutron logs for well 2-2A at the INEEL. 657  
 Stratigraphy for this well is based on examination of 2- 658  
 2A cores. Intraflow density changes in basalt are 659  
 measurable within most flows, grading from less-dense 660  
 vesicular basalt at flow boundaries to denser massive 661  
 basalt in flow interiors (see Fig. 6, feature A). Further- 662  
 more, the density contrast of basalt vs. interbed is 663  
 usually greater than the intraflow density contrast 664  
 (Fig. 6, feature B). Overall, the density contrast be- 665  
 tween the interbeds and the flows on Fig. 6 is sufficient 666  
 to identify flow and interbed boundaries. Combining 667  
 the gamma–gamma density log with a neutron log 668  
 makes these boundaries even more apparent. 669

670 Large voids like collapsed lava tubes can show up 670  
 on the gamma–gamma density log for the same 671  
 reasons they show up on the natural gamma log: there 672  
 are no significant particle interactions in void spaces. 673  
 On a density log, this results in less gamma flux 674  
 attenuation. When logging, depth intervals with high 675  
 counts on the gamma–gamma density log should be 676  
 re-examined on other logs, such as the natural gamma 677

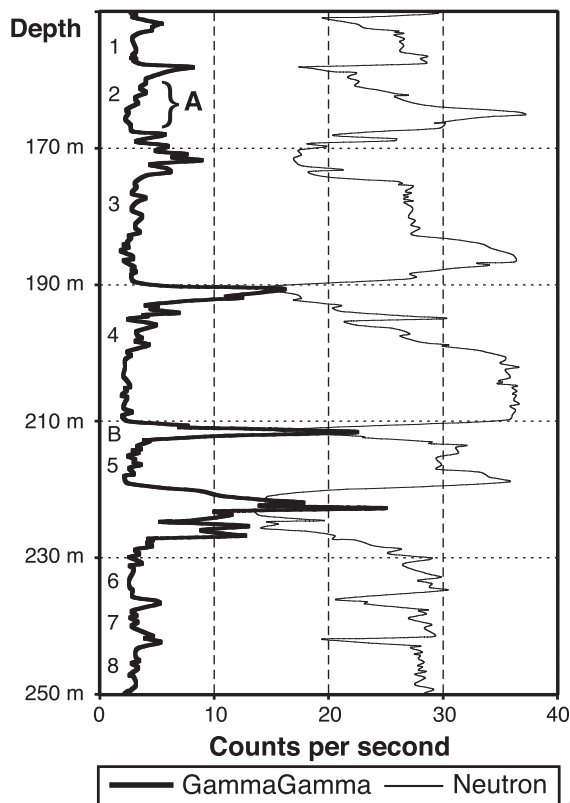


Fig. 6. Gamma–gamma density (left) and neutron (right) logs collected by the USGS in 1978 (Scott et al., 1979) from INEEL well 2-2A on the Eastern Snake River Plain. Well 2-2A is likely the most studied borehole on the East Snake River Plain, with multiple logs available of drill cuttings and core, plus an extensive suite of wireline logs. Individual basalt flows are numbered down the left margin of the figure. Feature A—the signature of a basalt flow grading from a more porous flow top to a dense massive flow interior, characterized by decreasing gamma flux on the gamma–gamma density log, indicating increase in density, plus increasing neutron flux, indicating decreasing porosity and/or hydrous minerals. Feature B—signature of an interbed, with elevated gamma flux on the gamma–gamma density, indicating decreased density, and low neutron counts, indicating increased porosity and/or hydrous minerals.

678 and caliper logs, for evidence of possible voids. In  
 679 Fig. 7, suspected voids (shaded intervals) in INEEL  
 680 well C1A are characterized by local maxima on the  
 681 gamma–gamma density log (i.e., by very little gamma  
 682 flux attenuation), indicative of lowered density.  
 683 Corresponding minima on the natural gamma log  
 684 support that these gamma flux peaks on the gam-  
 685 ma–gamma density log are caused by a textural and  
 686 not a compositional density drop. These log responses

687 correlate to two intervals of extensively fractured  
 688 basalt and basalt rubble in the C1A cores archived  
 689 by the United States Geological Survey (USGS).

### 15. Gamma–gamma density logs—problems of interpretation 690 691

692 The attenuated gamma flux of a gamma–gamma  
 693 density tool below the water table is significant when  
 694 compared to the attenuated flux in the unsaturated  
 695 zone, and this must be accounted for when correcting  
 696 a gamma–gamma log for borehole diameter and other  
 697 physical variables before attempting any quantitative  
 698 analysis for bulk density.

### 16. Geochemical logs 699

700 Geochemical logging is performed using nuclear  
 701 tool combinations incorporating various neutron and  
 702 gamma-ray sources, coupled with a variety of pas-  
 703 sive and activated gamma spectrum detectors. Mea-  
 704 suring the gamma energy spectrum is the backbone  
 705 of geochemical logging techniques. Since both pas-  
 706 sive gamma spectra and activated gamma spectra  
 707 can be resolved for emission contributions from  
 708 discrete elements, it is possible for a combination  
 709 of tools to measure relative major and trace element  
 710 concentrations at depth. For example, a neutron–  
 711 gamma log measures the gamma-ray emissions  
 712 caused by the capture of thermal neutrons. Each  
 713 element that can capture a thermal neutron will emit  
 714 gamma rays with characteristic energies specific for  
 715 that element, notably Ca, Cl, Fe, H, S, and Si  
 716 (Hertzog et al., 1988; Lamont-Doherty Earth Obser-  
 717 vatory, 2001). A variant of neutron–gamma logging  
 718 measures prompt gamma emissions caused instead  
 719 by the inelastic collision of fast neutrons with certain  
 720 elements, namely, Ca, C, Fe, O, S, and Si (Hertzog et  
 721 al., 1988; Lamont-Doherty Earth Observatory, 2001).  
 722 K, Th, and U concentrations can be determined by  
 723 measuring the natural gamma energy spectrum. The  
 724 variety of source and detector combinations is quite  
 725 large and describing them all is beyond the scope of  
 726 this study.

727 Through the use of a proprietary analysis tech-  
 728 nique, Schlumberger developed a means to measure

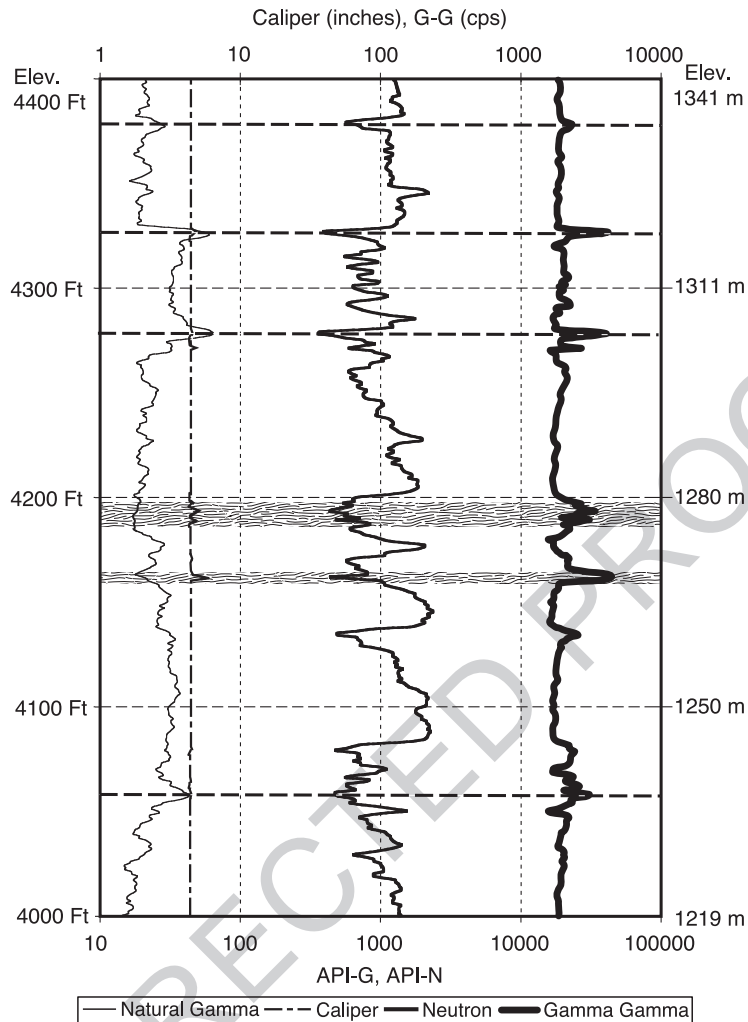


Fig. 7. Signature of void space in basalt for INEEL well C1A on the Eastern Snake River Plain. The caliper tool shows that the borehole has widened in the hatched intervals. The combination of lowered neutron flux plus lowered natural gamma counts argues that water in pores and fractures is the cause of the attenuated neutron flux, and not the presence of hydrous minerals. The combination of decreased gamma counts on the natural gamma log and increased gamma flux on the gamma–gamma density log indicates a decrease in density. C1A cores show that the hatched intervals are zones of fractured basalt and basalt rubble.

729 elemental abundances quantitatively in the 1980s. By  
 730 adding a gamma–gamma density log to measure  
 731 electron density and photoelectric capture cross section  
 732 (PEF), Mg concentration can be determined from  
 733 the difference between the measured and calculated  
 734 PEF based on the directly measured major elements  
 735 concentrations. Once all relative concentrations have  
 736 been measured or calculated, this information can be  
 737 incorporated into an oxide-closure model to deter-

mine abundances of major and trace elements, including K, Ca, Mg, Na, Fe, S, Ti, Si, Al, U, Th, and Gd (Herron and Herron, 1990; Hertzog et al., 1986; Hertzog et al., 1987). Schlumberger's proprietary method was originally developed for use in sedimentary rocks for petroleum exploration purposes, and the original oxide-closure models were based on elemental abundances representative of sedimentary environments.

738  
 739  
 740  
 741  
 742  
 743  
 744  
 745  
 746

747 **17. Geochemical logs—basalt applications**

748 The composition of basalt varies vertically between  
 749 flow groups (Wetmore, 1998) much more than it  
 750 varies laterally (cf. Bates, 1999). Geochemical logs  
 751 can discriminate, therefore, between flow groups and  
 752 can correlate flow groups between boreholes. Spectral  
 753 neutron–gamma logging has been used successfully  
 754 and extensively at the Pacific Northwest National  
 755 Laboratory (PNNL) in Washington State, in order to  
 756 characterize both rocks and contaminants in the sub-  
 757 surface at the PNNL, in both sediments and Columbia  
 758 River basalts (Last and Horton, 2000). Access to these  
 759 spectral neutron–gamma logs is limited, however,  
 760 since much of the PNNL data is published only in  
 761 PNNL internal documents.

762 The sedimentary-rock-based calibrations and ox-  
 763 ide-closure model originally developed for Schlum-  
 764 berger’s geochemical method are precise though not  
 765 accurate for several major elements when tested in  
 766 basalt by the ODP and closely related studies (Brewer  
 767 et al., 1989, 1990; Anderson et al., 1990a). Subse-  
 768 quently, successful calibrations and oxide-closure  
 769 models were developed for geochemical logging in  
 770 oceanic basalts as well as in other crystalline rocks  
 771 (Anderson et al., 1990a,b; Brewer et al., 1990; Drax-  
 772 ler, 1990).

773 **18. Geochemical logs—results and interpretations**

774 The ODP and other researchers have demonstrated  
 775 the usefulness of oxide-closure models for geochem-  
 776 ical logging in the oceanic environment and in con-  
 777 tinentals mafic rocks using Schlumberger’s original  
 778 suite of geochemical tools. Anderson et al. (1990b)  
 779 have demonstrated that their basalt-specific geochem-  
 780 ical log calibration and oxide-closure model gave  
 781 acceptable results in a small number of boreholes  
 782 dominated by continental mafic rocks in saturated  
 783 conditions. Though some studies like Bates (1999)  
 784 show that intraflow features in continental basalt  
 785 flows can have variable composition, most basalt  
 786 flows and flow groups do not vary significantly in  
 787 composition laterally (e.g., Buckley and Oliver, 1990;  
 788 Hooper, 1997; Hughes et al., 2002). It is clear,  
 789 therefore, that even the most complex geochemical  
 790 tool suites can be properly calibrated for basalt, and

should be able to distinguish between basalt flow 791  
 groups and interbeds by composition alone. Anderson 792  
 et al. (1990a,b) and Brewer et al. (1990) have pub- 793  
 lished detailed studies and reviews of geochemical 794  
 logging in mafic igneous rocks. 795

19. **Geochemical logs—problems of interpretation** 796

Neutron–gamma tools behave very differently 797  
 above the water table compared to below, as was 798  
 demonstrated by Crosby and Anderson (1971); this 799  
 effect is largely due to variations in  $L_s$  in saturated vs. 800  
 unsaturated conditions. Below the water table,  $L_s$  is 801  
 dominated by H, while above the water table,  $L_s$  is 802  
 much larger and more variable due to changes in 803  
 lithology. Since spectral neutron–gamma logs are a 804  
 very important component of geochemical logging 805  
 (Hertzog et al., 1987; Herron and Herron, 1990), tool 806  
 calibrations and oxide-closure models should be de- 807  
 veloped for unsaturated basalts. To date we know of 808  
 no basalt-specific calibrations and oxide-closure mod- 809  
 els available for unsaturated basalts. 810

Many geochemical wireline techniques can de- 811  
 liver qualitative elemental concentration measure- 812  
 ments in basalt. Quantitative results are possible 813  
 but depend on using tool calibrations which are 814  
 appropriate for mafic rocks. There are no tools “off- 815  
 the-shelf” calibrated for both saturated and unsatu- 816  
 rated basalt. Geochemical tools and methods that 817  
 are capable of measuring quantitative elemental 818  
 abundances in basalt have been either specialized 819  
 for use in very limited conditions, like at PNNL, or 820  
 are proprietary petroleum-exploration technology 821  
 with a large price tag attached. In addition, Schlum- 822  
 berger’s original geochemical tools have been 823  
 replaced by a second-generation tool suite which 824  
 utilizes recent advancements in germanium detectors. 825  
 Though the Schlumberger tools and oxide-closure 826  
 method can deliver the most versatile and accurate 827  
 results, the new generation of tools would require 828  
 recalibration and a new oxide-closure model before 829  
 they could be deployed. Geochemical logging in 830  
 basalt is currently limited by equipment and calibra- 831  
 tion issues, but this technique alone has the potential 832  
 to resolve basalt flow stratigraphy at the scale of 833  
 individual flows, without supplement from other 834  
 wireline tools. 835

836 **20. Resistivity logs**

837 Resistivity is essentially the inverse of conductivity. Most rock types are resistant to electric currents. 838  
 839 On the other hand, water is conductive compared to most earth materials, so when water is present in a 840  
 841 rock, it will dominate any resistivity measurements. 842  
 843 Assuming that resistivity response is a measure of water content, then resistivity in porous rocks can be 844  
 845 treated as a function of water-filled porosity, where the correlation equation between resistivity and water- 846  
 847 filled porosity is Archie's Law (Schlumberger, 1989). Resistivity is also useful in stratigraphic studies (e.g., 848  
 849 Versey and Singh, 1982) since different lithologies have differing resistivities. In addition, it is often 850  
 851 possible to use resistivity to identify thin zones of increased permeability: since permeable zones have 852  
 853 higher water content in saturated strata, it is often possible to identify these zones by comparing the 854  
 855 response of closely spaced "near" electrodes vs. more-separated "far" electrodes, where the former 856  
 857 will show a disproportionate decrease in conductivity compared to the latter (Goldberg, 1997).

858 **21. Resistivity logs—basalt applications**

859 Saturated basalt flows have a characteristic response on resistivity logs (e.g., Versey and Singh, 860  
 861 1982; Buckley and Oliver, 1990; Pezard, 1990). In general, resistivity is very high in the massive interiors 862  
 863 of basalt flows and low at flow breaks and in interbeds. This behavior is due to both porosity and compositional 864  
 865 changes between flows and interbeds. Most interbeds have lower resistivity compared to basalt, 866  
 867 since interbed sediments typically include more clays and other conductive minerals and are commonly 868  
 869 more porous than most basalts (Lovell and Pezard, 1990). Intraflow resistivity variations are governed 870  
 871 mostly by porosity changes. Flow interiors tend to have much lower porosity than flow boundaries, so the 872  
 873 amount of conductive fluid present is low and resistivity is high. Depending on the conductive fluid, the 874  
 875 uncorrected resistivity of flow interiors is usually greater than 1000  $\Omega$  m. Hence, a lateral or long/short 876  
 877 normal resistivity tool is preferred over an induction tool in basalt, since many of the former can handle the 878  
 879 extremely high resistivities encountered in the massive

interiors of basalt flows whereas most commercially available induction tools cannot (Goldberg, 1997). 880  
881

**22. Resistivity logs—results and interpretation** 882

883 Fig. 8 shows the lateral resistivity log for the first 250 m of the Hawaii Scientific Drilling Project 884  
 885 (HSDP) pilot hole, KP-1 (International Continental Drilling Program, 1999). KP-1 was continuously 886  
 887 cored; photographs and an annotated lithological log of the complete core suite are archived at the HSDP 888  
 889 web pages at the California Institute of Technology (Hawaii Scientific Drilling Project, 1993). The flows, 890  
 891 flow breaks, and interbeds shown in Fig. 8 are based on the lithological logs and unit descriptions from the 892  
 893 Hawaii Scientific Drilling Project (1993), Stolper et al. (1996), and Beeson et al. (1996). The KP-1 pilot 894  
 895 hole was drilled through the distal aprons of the Mauna Loa and Mauna Kea shield volcanoes where 896  
 897 the two overlap. The drilling site was immediately adjacent to the shoreline, and the water level in the 898  
 899 hole was  $\sim 30$  m bls when the hole was logged. There is no wireline data for the unsaturated zone of 900  
 901 KP-1. The KP-1 resistivity log shows a typical wireline behavior for a saturated basalt flow sequence: the 902  
 903 resistivity is high in the middle of flows, and low at flow breaks and interbeds. 904

905 Fig. 9 shows long/short normal resistivity logs for INEEL well C1A on East Snake River Plain, for 906  
 907 depths 0 to 400 m bls. The conductive fluid in the saturated basalts was potable water from the Snake 908  
 909 River Plain aquifer. Note that below the water table at 180 m, the resistivity data show the characteristic 910  
 911 high-resistivity humps expected in the middle of flows, separated by low-resistivity flow breaks and 912  
 913 interbeds. These resistivity features correlate strongly with flows and interbeds observed in the C1A cores. 914  
 915 In general, resistivity response below the water table is usually distinctive enough to discern flow stratigraphy 916  
 917 (e.g., Pezard, 1990; also see Fig. 8) and can sometimes be used to correlate basalt flows over 918  
 919 modest distances (Crosby and Anderson, 1971). 920

921 A polymer gel was added to C1A in an attempt to measure resistivity of unsaturated basalt. The resistivity 922  
 923 logs do not show the typical response of saturated basalt flows, i.e., resistant flow interiors vs. conductive 924  
 925 flow breaks and interbeds. For example, the 64-

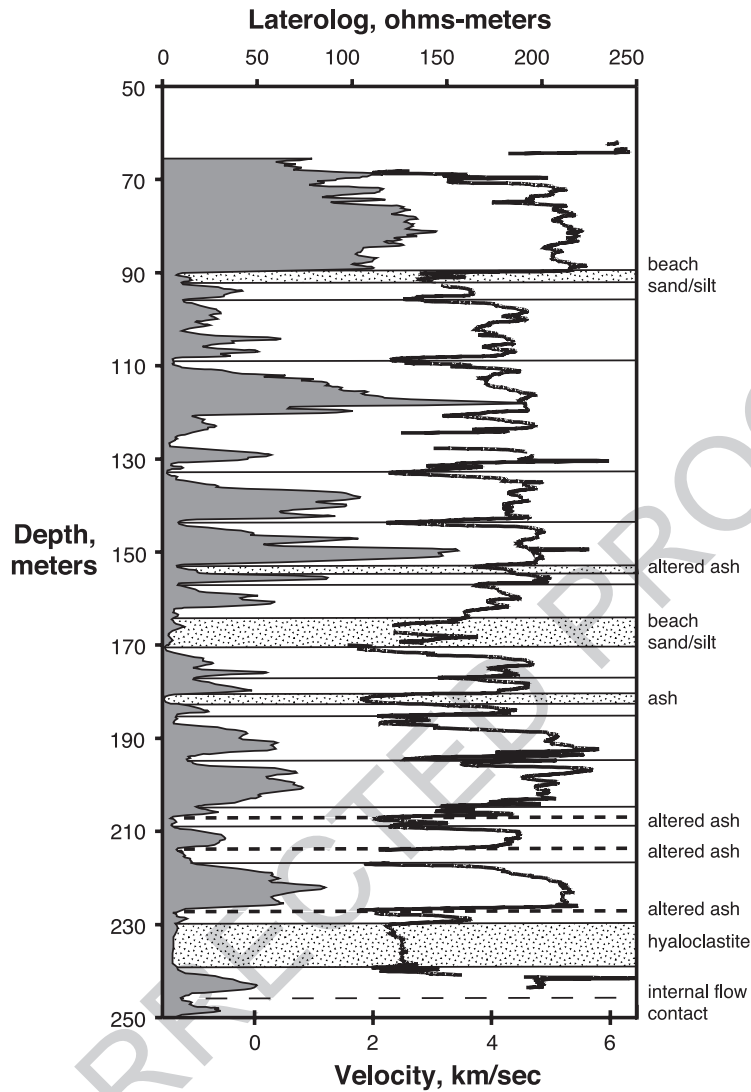


Fig. 8. Lateral resistivity and sonic velocity logs for the HSDP pilot hole KP-1. Both resistivity and velocity increase to the right. Basalt flow interiors are characterized by increased velocity and resistivity, whereas flow breaks are characterized by lowered velocity and resistivity. Data plotted is from the archive of HSDP logging results maintained by the International Continental Drilling Program (International Continental Drilling Program, 1999). Lithology based on cores is from Stolper et al. (1996) and Beeson et al. (1996).

925 in. (162.6 cm) long normal resistivity log is significantly different from the 16-in. (40.6 cm) short normal resistivity log at depths between  $\sim 40$  and  $\sim 75$  m bls, and again at  $\sim 175$  m bls. One viable explanation is that the resistivity behavior is indicative of resistivity reversals, which happen when a layer is thinner than the long electrode spacing but thicker than the short electrode spacing (Schlumberger, 1989). In a

933 resistivity reversal, a resistant thin layer will cause 933  
 934 decreasing resistivity on the long normal resistivity 934  
 935 log, but increasing resistivity on the short normal 935  
 936 resistivity log, causing the two measurements to 936  
 937 diverge. Examples of this can be seen in Fig. 9 937  
 938 between 40 and 75 m. Cores from C1A between 40 938  
 939 and 75 m are highly fractured, brecciated, and/or 939  
 940 oxidized in layers commonly thinner than 64 in. 940

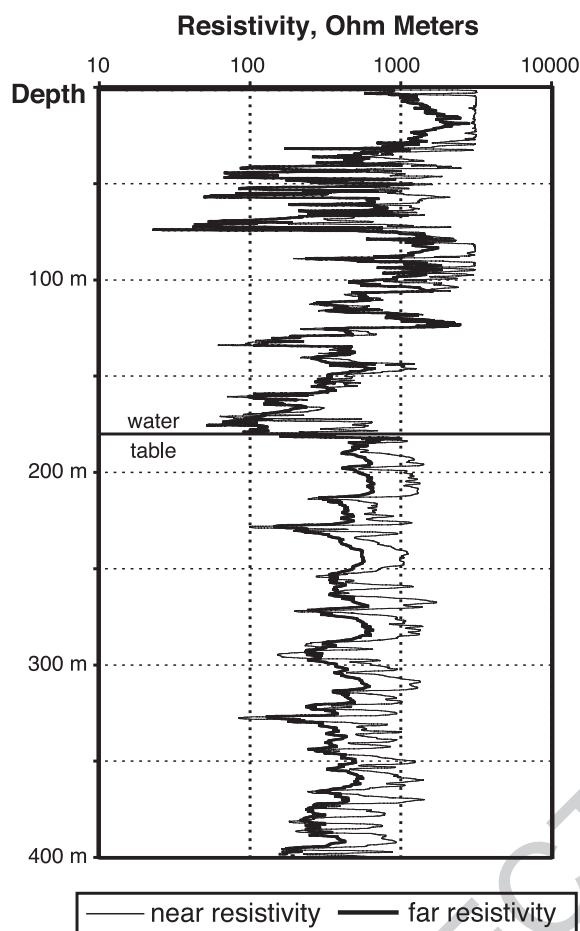


Fig. 9. Long and short normal resistivity logs for a portion of INEEL well C1A. Resistivity increases to the right. Electrode spacings are at 64 in. (162.6 cm) and 16 in. (40.6 cm). Depth to the water table is ~180 m bls. Below the water table, the data show the characteristic high-resistivity humps typical of the massive interiors of basalt flows, separated by low-resistivity flow breaks and interbeds. A polymer gel was added to the borehole in the unsaturated zone in order to log resistivity above the water table.

941 (162.6 cm), so the reversal of the 64-in. (162.6 cm)  
 942 normal resistivity is possible. Another example of  
 943 resistivity reversal is shown in Fig. 10, for basalt in  
 944 INEEL well 2-2A. Though the original researchers at  
 945 2-2A collected data for 4-in. (10.2 cm), 8-in. (20.3  
 946 cm), 16-in. (40.6 cm), 32-in. (81.3 cm), and 64-in.  
 947 (162.6 cm) electrode spacings (P. Nelson, pers.  
 948 comm.), only the 16-in. (40.6 cm) and 64-in. normal  
 949 resistivity logs (162.6 cm) were published (Scott et  
 950 al., 1979).

### 23. Resistivity logs—problems of interpretation

951

Basalt is one of the most resistive rocks, and many  
 commercially available resistivity tools are inadequate  
 for measuring its extremely high resistivity (e.g.,  
 Blackwell et al., 1982; Priest et al., 1982; also see  
 Fig. 9, 0 to 30 m bls). In general, traditional resistivity  
 logs (excluding induction) are not used in dry holes,  
 since resistivity measurements depend on the existence  
 of a closed circuit between electrodes. A closed  
 circuit is usually achieved by the presence of a  
 conductive fluid in the borehole like drilling mud or  
 water. In an air-filled borehole, a closed circuit is not  
 possible since air is not conductive.

952  
953  
954  
955  
956  
957  
958  
959  
960  
961  
962  
963

There are three potential ways to measure resistivity  
 in unsaturated basalts. The first is to add a conductive  
 fluid, like the polymer gel used in INEEL well C1A.  
 Adding such fluids to a well, however, is often  
 problematic in areas of degraded ground water and  
 heightened regulatory oversight. In addition, such  
 fluids usually break down within hours or days of  
 their injection into a borehole, limiting the window of  
 opportunity to perform resistivity logging. The second  
 way to measure resistivity in a dry hole is to create a  
 circuit by pressing the electrodes against the borehole  
 wall (e.g., Crosby and Anderson, 1971), though in  
 basalt, the frequently uneven nature of the borehole  
 wall may preclude the use of such tools. The third way  
 to log a dry hole would be to use an induction log.  
 Most induction tools are traditionally limited to high-  
 conductivity environments, commonly  $<100 \Omega \text{ m}$   
 (Schlumberger, 1989), and will not respond in very  
 high-resistivity rocks like basalt (Goldberg, 1997).  
 The experience of the Mt. Hood geothermal project is a  
 good example of the unresponsiveness of an induction  
 tool in basalt flows (Blackwell et al., 1982). In general,  
 a resistivity tool that establishes a physical closed  
 circuit between electrodes is preferred over an induction  
 tool in basalt, since the former can usually handle  
 extremely high resistivity measurements (Goldberg,  
 1997). Unlike induction tools, however, traditional  
 normal and lateral resistivity tools require the presence  
 of a conductive fluid in the borehole.

964  
965  
966  
967  
968  
969  
970  
971  
972  
973  
974  
975  
976  
977  
978  
979  
980  
981  
982  
983  
984  
985  
986  
987  
988  
989  
990  
991  
992

Porosity in sedimentary rocks can be calculated  
 from resistivity using Archie's law, but using Archie's  
 law for basalts is problematic (e.g., Becker et al.,  
 1982). It assumes that any contribution by conductive  
 clays is negligible. Using Archie's Law when con-

993  
994  
995  
996  
997

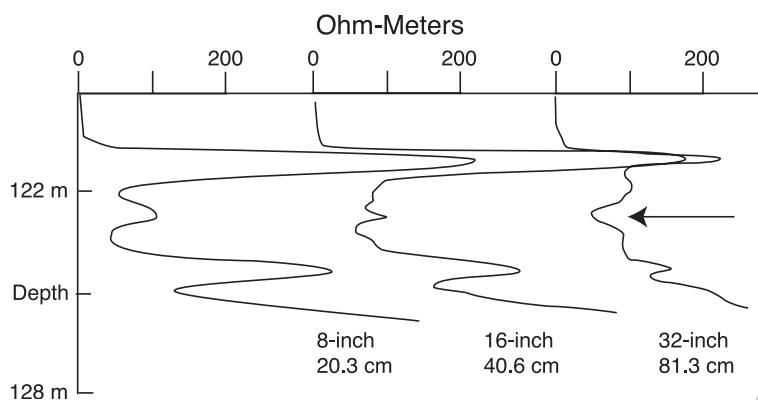


Fig. 10. Three normal resistivity measurements in saturated basalt using electrodes at spacings of 8 (20.3 cm), 16 (40.6 cm) and 32 (81.3 cm) in. The arrow marks the location of a resistivity reversal for a layer less than 32 in. (81.3 cm) thick. This data for INEEL well 2-2A was collected by the USGS in 1978 (P. Nelson, pers. comm.).

998 ductive clay minerals are present can result in porosity  
 999 calculations which are too high. For rocks with  
 1000 typically low permeability, like amygdaloidal basalt,  
 1001 this juxtaposition of high apparent porosity vs. low  
 1002 permeability is the “apparent porosity paradox” dis-  
 1003 cussed by Pezard (1990) and other DSDP/ODP  
 1004 researchers. There have been attempts to generate  
 1005 valid variations of Archie’s Law for basalt (e.g.,  
 1006 Pezard, 1990; Becker et al., 1982) to account for  
 1007 alteration and conductivity in cracks and microcracks,  
 1008 with mixed success. Without a good estimate of the  
 1009 concentration and composition of conductive alter-  
 1010 ation minerals, however, any sort of correction  
 1011 scheme will be doubtful.

## 1012 24. Velocity logs

1013 Velocity logs, also known as sonic logs or acoustic  
 1014 logs, measure the travel time of an acoustic pulse. Most  
 1015 modern sondes are equipped with one or more pulse  
 1016 transmitters and two or more detectors a short distance  
 1017 away. Two of the principal uses of velocity logs are to  
 1018 calculate porosity and to identify fracture zones  
 1019 (Schlumberger, 1989). Fracture zones can be identified  
 1020 by increased travel time for the pulse to reach the  
 1021 detector(s). Porosity can be calculated using the Wyllie  
 1022 time-average equation (Schlumberger, 1989; Keys and  
 1023 MacCary, 1971), whose inputs are measured travel  
 1024 time,  $\Delta t$ , and assumed velocities for both the borehole  
 1025 fluid and the rock matrix,  $V_f$  and  $V_m$ , respectively.

Given the measured  $\Delta t$  for an interval, a reasonable  
 value for porosity can be calculated.

## 25. Velocity logs—basalt applications

Velocity logs in basalt act no differently than  
 velocity logs in other rocks. There are two items of  
 interest, however, for velocity logs in basalt. The first  
 is the determination of porosity based on measured  
 velocity and travel times. As already discussed, other  
 logs commonly used to calculate porosity, i.e., resis-  
 tivity and neutron logs, can overestimate porosity  
 when hydrous minerals are present. Velocity logs,  
 however, are independent of neutron moderation and  
 increased conductivity, the properties which introduce  
 an excess porosity error for neutron and resistivity  
 logs, respectively. The porosity derived from velocity  
 logs is the effective porosity, i.e., the interconnected  
 porosity through which fluids can travel. Secondary  
 porosity, i.e., the unconnected pore spaces of unfilled  
 vesicles, vugs, and fractures, is not measured, since  
 the propagating acoustic pulse does not “see” these  
 void spaces, but will travel around them through the  
 solid matrix of the rocks in the borehole (Schlum-  
 berger, 1989).

The other item of interest is the distinctive pattern  
 of velocity variations made by lower-velocity flow  
 breaks and interbeds which separate higher-velocity  
 flow interiors. This pattern is useful for locating  
 flows, flow breaks, and interbeds in the subsurface.

## 1054 26. Velocity logs—results and interpretation

1055 Fig. 8 shows a resistivity and velocity log for the  
1056 KP-1 on Hawaii (International Continental Drilling  
1057 Program, 1999). Like resistivity, acoustic velocity is  
1058 high in the massive interior of flows and low at flow  
1059 breaks and interbeds. Velocity drops in the interbeds  
1060 and flow breaks due to increased fracturing at flow  
1061 boundaries and the less cohesive nature of the inter-  
1062 beds compared to flow interiors. This pattern of  
1063 velocity variation seems to present in most basalt flow  
1064 sequences where velocity logs have been collected.

## 1065 27. Velocity logs—problems of interpretation

1066 A fracture zone in the interior of a flow cannot be  
1067 distinguished from a flow break by using a velocity  
1068 log alone, since both phenomenon will cause in-  
1069 creased travel times for the acoustic pulse. If a fracture  
1070 zone is not infilled with sediment, then it may be  
1071 possible to correctly identify it if the natural gamma  
1072 log is constant through the zone in question. If the  
1073 fracture zone is unaltered and/or unsaturated, then  
1074 magnetic susceptibility and neutron logs will also be  
1075 constant through the fractured interval.

## 1076 28. Magnetic susceptibility logs

1077 When any material is exposed to a magnetic field  $H$ ,  
1078 it acquires an induced magnetization  $J$  (following the  
1079 symbol and unit conventions of Butler, 1992). The  
1080 magnitude of  $J$  is related to the applied field  $H$  by a  
1081 dimensionless proportionality constant,  $\chi$ , known as  
1082 the magnetic susceptibility, such that  $J = \chi H$ . Magnetic  
1083 susceptibility is essentially a measure of how strongly a  
1084 material can be magnetized (Butler, 1992; Dunlop and  
1085 Ozdemir, 1997). In borehole geophysics, magnetic sus-  
1086 ceptibility is measured on a volume basis (e.g., Nelson,  
1087 1993). The units for  $\chi$  are dimensionless and are  
1088 commonly reported as  $\mu\text{SI}$ ,  $\text{mSI}$ , or  $\text{SI}$  units. Units of  
1089  $\mu\text{SI}$  are most common since the magnetic susceptibility  
1090 of most earth materials is  $\sim 10^{-6}$  SI (Dean, 1995).

1091 Magnetic susceptibilities for the ferromagnetic  
1092 minerals, i.e., minerals which can carry remanent  
1093 magnetization, are greater by several orders of mag-  
1094 nitude than most other earth materials (Butler, 1992;

Dean, 1995). When present, ferromagnetic minerals 1095  
will dominate the magnetic susceptibility of any rock. 1096  
For this reason, magnetic susceptibility tools are 1097  
designed and calibrated for use in rocks containing 1098  
ferromagnetic minerals. This is actually of great utility 1099  
since some of the most common rock-forming min- 1100  
erals are ferromagnetic, including magnetite and he- 1101  
matite. Goethite and hematite typically have magnetic 1102  
susceptibilities less than  $100 \mu\text{SI}$ , though in some 1103  
cases,  $\chi$  can be as high as  $250 \mu\text{SI}$  for goethite and as 1104  
high as  $1000 \mu\text{SI}$  for hematite (Clark and Emerson, 1105  
1991; Butler, 1992; Dunlop and Ozdemir, 1997). In 1106  
comparison, the magnetic susceptibility of magnetite 1107  
ranges from  $\sim 10,000$  to  $\sim 3,000,000 \mu\text{SI}$  (Clark and 1108  
Emerson, 1991; Dunlop and Ozdemir, 1997). 1109

Magnetic susceptibility in ferromagnetic minerals 1110  
depends on factors such as magnetic domain size, the 1111  
amount of titanium substitution for iron, the oxidation 1112  
history of the magnetic minerals, etc. Dunlop and 1113  
Ozdemir (1997) present perhaps the most current and 1114  
comprehensive discussion of factors effecting mag- 1115  
netic susceptibility in minerals. In general, oxidizing 1116  
magnetite to hematite will cause susceptibility to drop 1117  
by two more orders of magnitude, which is not 1118  
uncommon for weathered soil horizons (Butler, 1119  
1992), gossans, or economic mineralization of sedi- 1120  
mentary rocks (Scott et al., 1981, 1983). Nelson 1121  
(1993) reviewed the application of magnetic suscep- 1122  
tibility logging in sedimentary rocks and tuffaceous 1123  
volcanoclastic sequences, noting that in some cases, 1124  
magnetic susceptibility logs were effective in resolv- 1125  
ing stratigraphic correlations over ones of kilometers. 1126  
Fukuma (1998) was able to correlate magnetic suscep- 1127  
tibility peaks in oceanic sediments between ODP 1128  
holes over 50 km apart. 1129

## 29. Magnetic susceptibility logs—basalt 1130 applications 1131

Since magnetite is an important accessory mineral 1132  
in basalt, basalt is one of the most highly magnetized 1133  
rocks, with  $\chi$  values typically greater than  $100 \mu\text{SI}$ . 1134  
Properties which are sensitive to  $\chi$  in basalt are both 1135  
compositional and textural. The initial  $\chi$  for any given 1136  
basalt flow is a function of magnetite grain size, 1137  
which is governed by cooling history, by the amount 1138  
of magnetite present in the rock, and by the amount of 1139

1140 titanium substitution in the magnetite (Dunlop and  
 1141 Ozdemir, 1997). Post-emplacment changes of  $\chi$  in  
 1142 basalt are commonly due to the oxidation of magnetite  
 1143 to predominantly hematite plus some ilmenite and  
 1144 other minor oxides (Butler, 1992; Dunlop and Ozde-  
 1145 mir, 1997). Secondary stratigraphic features, such as  
 1146 sedimentary interbeds between flows, will typically  
 1147 show up on magnetic susceptibility logs as zones of  
 1148 lowered magnetic susceptibility.

### 30. Magnetic susceptibility logs—results and interpretation

Fukuma (1998) analyzed magnetic susceptibility in  
 oceanic sediments and submerged, originally subaerial  
 basalts as part of ODP Leg 152, to study the nature of  
 the rifted margin off of southeast Greenland. While  
 there are many ODP and other studies on magnetic  
 susceptibility, Fukuma's (1998) study is a good exam-

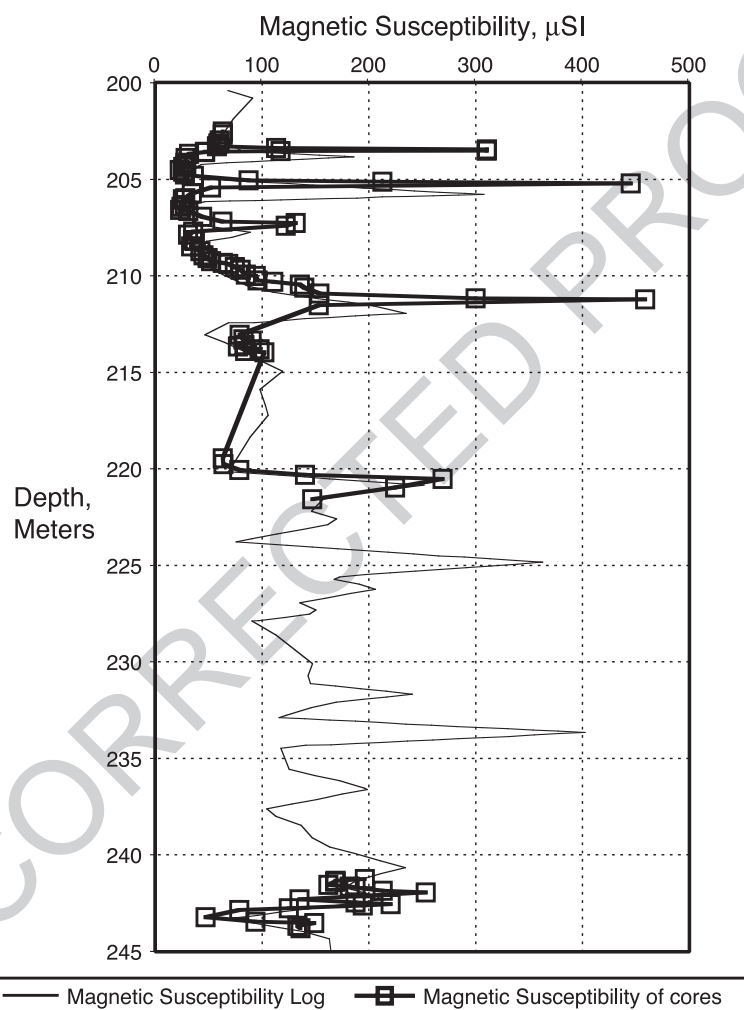
1149  
11501151  
1152  
1153  
1154  
1155  
1156

Fig. 11. Magnetic susceptibility log (thin line, no data point markers) collected in the field (Scott et al., 1979) and magnetic susceptibility data (thick line with data point markers) measured on sample cores by the USGS in 1978 (P. Nelson, pers. comm.) for a portion of INEEL well 2-2A on the Eastern Snake River Plain. No depth corrections were applied since it is easier to compare the two data sets with the small depth offset present. The discrepancy exists because the discrete-sample depths were referenced to the ground surface, whereas a hand annotation on the original 1979 paper logs indicates that the log depths were referenced to the top of the well casing, 0.4 m above the ground surface. The complete magnetic susceptibility log for this borehole is shown in Fig. 12.

1157 ple of how several different physical properties can  
 1158 affect the measurement of  $\chi$  in basalt. The basalts  
 1159 studied by Fukuma behaved as follows: fine-grained  
 1160 scoriaceous basalt at the top of flow units typically had  
 1161 magnetic susceptibilities 2 to 10 times greater (20 to 50  
 1162  $\mu\text{SI}$ ) than basalt flow interiors ( $\sim 5$  to  $10 \mu\text{SI}$ ). Some  
 1163 of the fine-grained scoriaceous basalt did not have  
 1164 elevated  $\chi$  values ( $< 1 \text{ mSI}$ ) where it was oxidized.  
 1165 Fukuma (1998) specifically noted that the baseline  $\chi$  of

1166 flow interiors from different flow series [sic] was  
 1167 controlled by the original composition of unaltered  
 1168 magnetites. Using this information, Fukuma was able  
 1169 to differentiate picritic basalts ( $\sim 2000 \mu\text{SI}$ ) from  
 1170 more evolved basalts and dacites ( $\sim 4000 \mu\text{SI}$ ).  
 1171

1172 Fukuma's (1998) measurements reveal some inter-  
 1173 esting characteristics of magnetic susceptibility in  
 1174 basalts. Magnetic susceptibility in very fine-grained,  
 1175 quickly cooled scoriaceous flow tops was generally  
 1176

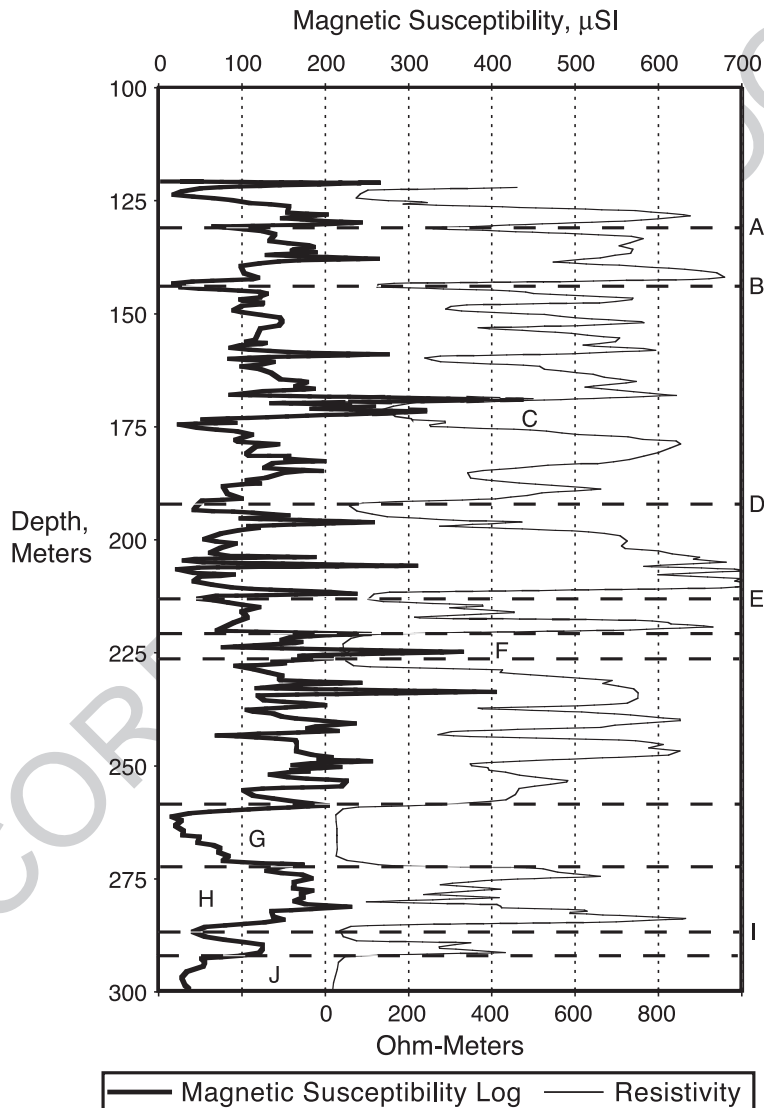


Fig. 12. Magnetic susceptibility and near (16-in./40.6 cm) resistivity logs in basalt for INEEL well 2-2A on the Eastern Snake River Plain (Scott et al., 1979). Lettered features explained in the text.

1175 higher than in flow interiors. This is in keeping with  
 1176 the well-known property of quickly cooled magnetite  
 1177 for preserving magnetic remanence, due to the pre-  
 1178 dominance of small magnetite grains carrying a single  
 1179 magnetic domains (Butler, 1992). The lower magnetic  
 1180 susceptibility of the flow interiors can be interpreted  
 1181 as the consequence of longer cooling times, leading to  
 1182 larger magnetite grains which carry less-effective  
 1183 multiple magnetic domains (Butler, 1992). Fukuma's  
 1184 (1998) susceptibility results also show that where  
 1185 basalts had been oxidized and ferrous iron minerals  
 1186 were altered to ferric ones,  $\chi$  dropped typically two  
 1187 orders of magnitude, which is well within the mag-  
 1188 netic susceptibility range for hematite. While Fuku-  
 1189 ma's (1998) measurements were made on discrete  
 1190 sample cores collected during drilling. Fukuma  
 1191 remarked that in situ magnetic susceptibility recorded  
 1192 with a wireline tool would have been preferable and  
 1193 would have had the advantage of delivering a contin-  
 1194 uous record with no data gaps.

1195 Scott et al. (1979) collected a ~ 200-m magnetic  
 1196 susceptibility log in subsurface sediments and basalts  
 1197 in well 2-2A at the INEEL. They also collected  
 1198 discrete samples from the 2-2A cores which were  
 1199 subsequently measured for magnetic susceptibility in  
 1200 the lab (P. Nelson, pers. comm.). Fig. 11 shows a  
 1201 portion of the magnetic susceptibility log plotted with  
 1202 the susceptibility measurements made on the discrete  
 1203 samples from well 2-2A. Overall, the correlation of  
 1204 the log and the lab measurements is good. Three of the  
 1205 discrete-sample susceptibility peaks are much greater  
 1206 than the corresponding peaks on the continuous log,  
 1207 though the lower susceptibility values appear to  
 1208 correlate well. The reason for the mismatch of peaks  
 1209 is not known, though it may be the consequence of  
 1210 different susceptibility bridge configurations used in  
 1211 the lab and the field, different sample volumes, or a  
 1212 bad calibration of either the wireline tool or the  
 1213 laboratory susceptibility bridge. The depth interval  
 1214 plotted on Fig. 11 is a subset of the magnetic suscep-  
 1215 tibility log for well 2-2A shown in Fig. 12.

### 1216 31. Magnetic susceptibility—potential problems of 1217 interpretation

1218 Fig. 12 shows the magnetic susceptibility log and  
 1219 the 16-in. (40.6 cm) resistivity log collected by Scott

et al. (1979). It is quickly apparent that there is more  
 detail in the magnetic susceptibility log than can be  
 correlated with details on the resistivity log. This is  
 due to the fact that variations in magnetic susceptibil-  
 ity do not always reflect primary compositional or  
 textural features such as flow breaks or magnetite  
 abundance. This can be shown by correlating the  
 lithology of well 2-2A cores to features on the logs  
 (Doherty, 1979; Blair, 2002; Anon., unpubl. data,  
 1978–2002, archived at INEEL HDR).

Features A, B, D, E, and I mark the location of thin  
 sedimentary interbeds characterized by low resistivity.  
 Each of these is also associated with decreased mag-  
 netic susceptibility, indicative that there are either no  
 ferromagnetic minerals present, or that any magnetic  
 minerals present are highly oxidized. In general, flow  
 interiors have background magnetic susceptibilities an  
 order of magnitude greater than those of the thin  
 interbeds. Features G and J are thick sequences of  
 silty clay, both with lowered resistivity and magnetic  
 susceptibility. This interbed pattern, however, is not  
 consistent; for example, feature F is an interbed layer  
 of both silty clay and sand. Feature C is a wide layer  
 of lowered resistivity, but with several magnetic  
 susceptibility peaks. The lithological log of the bore-  
 hole (Doherty, 1979) describes the region from 143 to  
 192 m as one flow group with six individual flows  
 and no interbeds. The basalt of the flow group is  
 logged as highly fractured. Above feature C, the upper  
 four flows are described as being oxidized and dis-  
 colored with “iron-oxide staining.” The flows below  
 C are still highly fractured but are not described as  
 being oxidized or altered. Overall, the flow breaks  
 correspond to regions of higher magnetic susceptibil-  
 ity and lowered resistivity. At feature C, the basalt is  
 fractured and hosts two closely spaced flow breaks.  
 The magnetic susceptibility peaks may represent  
 quickly cooled fine-grained basalt at flow tops and  
 bottoms, similar to the flow margins examined by  
 Fukuma (1998), and/or tool response artifacts due to  
 thinly bedded and fractured flows (Nelson, 1993).

Feature H on Fig. 12 is similar to the situation at C;  
 however, the flow group here not only hosts several  
 individual flows, but also four very thin silty clay  
 interbeds (C. Whitaker, pers. comm.; Doherty, 1979).  
 These interbeds show up on the resistivity log much  
 more clearly than on the magnetic susceptibility log. In  
 this case, none of the sedimentary interbeds is associ-

1268 ated with a decrease in susceptibility, arguing that  
 1269 unoxidized ferromagnetic minerals are present, or that  
 1270 the flows and interbeds are thinly bedded. Though the  
 1271 potential for stratigraphic correlation is great (e.g.,  
 1272 Fukuma, 1998), magnetic susceptibility logs in basalt  
 1273 should be interpreted in tandem with other log types to  
 1274 identify otherwise confusing intraflow features.

### 1275 32. Magnetic polarity logs

1276 It is a valid first-order approximation to treat the  
 1277 Earth's magnetic field as a dipole. This dipole is not  
 1278 aligned perfectly with the Earth's rotational axis, but  
 1279 rather wobbles around the rotational axis along a  
 1280 random walk pathway (Butler, 1992). If a remanent  
 1281 magnetization forms quickly in a rock, over a few  
 1282 days or months for most basalts, then all the magnetic  
 1283 moments will point in the direction of the magnetic  
 1284 dipole axis with only a small amount of scatter. If  
 1285 magnetic remanence directions are averaged over  
 1286 periods of 2000 or more years, the averaged direction  
 1287 toward the magnetic dipole axis will be parallel to the  
 1288 Earth's rotational axis. As a tectonic plate moves,  
 1289 remanence directions will point towards the magnetic  
 1290 dipole axis which appears to wander away from the  
 1291 Earth's rotation axis in the reference frame of the  
 1292 tectonic plate. If the layers in a sequence each formed  
 1293 quickly, then the direction of the magnetic moments  
 1294 for any given layer will be approximately the same  
 1295 regardless of where that layer was sampled. It is  
 1296 possible, therefore, to make stratigraphic correlations  
 1297 based on matching remanence directions.

1298 The Earth's magnetic field changes polarity on a  
 1299 scale of  $10^5$  to  $10^6$  years. Magnetic remanence records  
 1300 polarity at the time it was acquired. By dating the  
 1301 periods of normal and reversed polarity, it is possible  
 1302 to construct a geomagnetic polarity timescale (GPT).  
 1303 If the pattern of polarity reversals from a sequence of  
 1304 rocks can be matched to a portion of the GPT, then  
 1305 that sequence can be dated paleomagnetically. During  
 1306 a logging program, if a polarity reversal is known or  
 1307 suspected for the rocks in the borehole, it is some-  
 1308 times possible to map that reversal in the subsurface  
 1309 using a magnetometer tool. Correlating the location of  
 1310 paleomagnetic reversals in boreholes is another pow-  
 1311 erful paleomagnetic technique for establishing subsur-  
 1312 face stratigraphy.

### 33. Magnetic polarity logs—application and interpretation

1315 There are several different approaches to determine  
 1316 magnetic polarity with a borehole magnetometer. The  
 1317 most rigorous requires a combination of a gyroscopic  
 1318 orientation tool plus a three-component magnetometer  
 1319 (Salisbury et al., 1986). A three-component magne-  
 1320 tometer tool contains three orthogonal magnetometers  
 1321 which measure two horizontal and one vertical com-  
 1322 ponents. Since all unclamped tools rotate in the  
 1323 borehole, an independent means of determining ori-  
 1324 entation is required, such as a gyroscopic orientation  
 1325 tool. A magnetometer alone should not be used to  
 1326 determine tool orientation since magnetic anomalies  
 1327 in the borehole can cause deflections in the measured  
 1328 directions.

1329 Once the magnetometer tool has measured magne-  
 1330 tization in a borehole, the data must be processed to  
 1331 convert the measurements to a north/east/vertical  
 1332 coordinate system and to remove the effects of the  
 1333 Earth's magnetic field, the induced field of the well  
 1334 casing if present, and the induced field of the rocks  
 1335 and fluids in the borehole (Salisbury et al., 1986). The  
 1336 magnetic susceptibility of the materials in the bore-  
 1337 hole must be measured or estimated, since without  
 1338 this knowledge, it is impossible to calculate the  
 1339 induced field. Assuming that all the corrections can  
 1340 be made, then the leftover post-correction magnetiza-  
 1341 tion should be the remanence, where the polarity is  
 1342 determined by the direction of the vertical component.  
 1343 Salisbury et al. (1986) obtained good results using this  
 1344 methodology on oceanic basalts.

1345 Scott and Olsen (1985) developed a different  
 1346 method for use with a three-component magnetom-  
 1347 eter. Completely skirting the issue of corrections  
 1348 for the induced field, polarity was estimated based  
 1349 on the deflection of the vertical component of  
 1350 magnetization with respect to true vertical measured  
 1351 with a gyroscope, where positive anomalies corre-  
 1352 lated with reversed polarity and negative anomalies  
 1353 with normal polarity. Scott and Olsen (1985)  
 1354 obtained good results using this method in volcanic  
 1355 rocks in south central Nevada. This method is similar  
 1356 to that used by Kuehn (1995), who employed a  
 1357 portable fluxgate magnetometer to find polarity rever-  
 1358 sals in Columbia River Plateau basalts exposed in  
 1359 outcrops.

### 1360 34. Magnetic polarity logs—potential problems of 1361 interpretation

1362 Magnetic polarity logs in basalt are uncommon.  
1363 While there are many three-component magnetometer  
1364 tools available for mineral exploration and borehole  
1365 deviation purposes, there are few tools specifically  
1366 adapted for magnetic polarity logging in basalt. Some  
1367 magnetic tools are not adequate for use in strongly  
1368 magnetized rocks such as basalt, like the Schlum-  
1369 berger-operated specialty tool currently on the OPD  
1370 ship *Joides Resolution* (D. Goldberg, pers. comm.).  
1371 Many borehole deviation tools which use magneto-  
1372 meters for orientation may be adaptable for use in  
1373 basalt, though without the addition of a gyroscopic  
1374 and/or accelerometer-dependent orientation tool, any  
1375 magnetic orientations collected in strongly magne-  
1376 tized contiguous basalt flows will be meaningless  
1377 except for possibly the vertical component.

### 1378 35. Temperature logs

1379 Temperature logging in boreholes which penetrate  
1380 continental basalt provides a wide variety of informa-  
1381 tion, including crustal geothermal gradient and heat  
1382 flow (Blackwell and Steele, 1992), effects of aquifer  
1383 flow on subsurface temperatures (Ziagos and Black-  
1384 well, 1981; Swanberg et al., 1988; Bartolino and  
1385 Niswonger, 1999), long-term climatic temperature  
1386 changes (Harris and Chapman, 1997; Pollack et al.,  
1387 1998; Skinner and Majorowicz, 1999; Majorowicz et  
1388 al., 1999), and the mechanics of fault zones (Brune et  
1389 al., 1969; Lachenbruch and Sass, 1980). In addition,  
1390 Williams and Anderson (1990) reviewed borehole  
1391 geophysical methods for estimating heat flow in both  
1392 oceanic and continental basalts in a wide variety of  
1393 settings.

### 1394 36. Temperature logs—basalt applications

1395 Temperature logging on the Snake River Plain  
1396 possibly represents the largest body of work of this  
1397 type thus far conducted in basalts. This research  
1398 program has mostly been directed at determination  
1399 of crustal heat flow and gross characteristics of the  
1400 Snake River Plain aquifer (Brott et al., 1981; Black-

well, 1989). This work has shown that the conductive  
heat flow is significantly higher than that of the  
surrounding Basin and Range province and that the  
rapid movement of cold ground water in Snake River  
Plain aquifer strongly affects near-surface tempera-  
tures and heat flow. In most places boreholes must be  
several hundred meters deep in order to penetrate  
beneath the effects of the aquifer and provide a true  
estimate of the regional conductive gradient and heat  
flow (see Fig. 13). For such deep wells, temperature  
profiles show a pronounced inflection at the base of  
the actively flowing cold waters of the aquifer and  
allow mapping of the aquifer thickness on parts of the  
INEEL.

Recent work with temperature logs at INEEL is  
focused on mapping aquifer temperature variations to  
define groundwater flow paths. This is possible  
because temperature of water varies depending on  
its sources. Much of the aquifer water passing  
through the INEEL area has been warmed by the  
high heat flow from the underlying crust to temper-  
atures of 11 to 13 °C. This contrasts sharply with  
cold recharge water (7 to 9 °C) from drainages north  
of the Plain, and with anomalously warm zones (up  
to 18 °C at the water table) where geothermal heat  
and fluids from depth have affected the aquifer.  
Current efforts are directed at mapping temperature  
contours in the aquifer at various depths in an area  
100 km by 50 km along the northern boundary of the  
central Eastern Snake River Plain (R.P. Smith, pers.  
comm.).

### 37. Temperature logs—results and interpretations

Work with temperature logs of wells in the East  
Snake River basalts has produced the following  
results.

1. The rapidly flowing cold waters of the Snake  
River Plain aquifer, recharged by high altitude snow-  
melt, mask the high heat flow of the eastern Snake  
River Plain. This situation is similar to high-heat flow  
masking by cold meteoric recharge waters in the  
actively volcanic Cascade Range described by Swan-  
berg et al. (1988).

2. The aquifer beneath the INEEL ranges in thick-  
ness from less than 100 m to about 400 m, similar to  
aquifer thickness on the Columbia River Plateau in

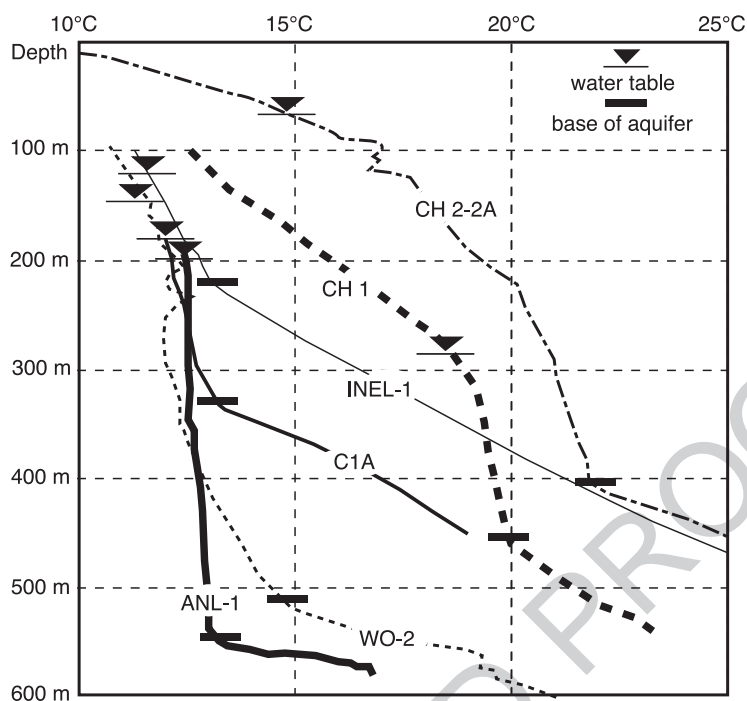


Fig. 13. Temperature profiles of deep wells in basalt flows on the Eastern Snake River Plain. This figure shows typical profiles of temperature gradient above, in, and below the basalt-hosted Snake River Aquifer. Profiles are best exemplified by the temperature log traces for INEEL wells 1 and 2-2a (labeled “CH 1” and “CH 2-2A”). The aquifer corresponds to the portion of the log traces with the lower temperature gradient, and the unsaturated and subaquifer zones by the much higher temperature gradients.

1446 northwestern Washington State (Crosby and Ander-  
 1447 son, 1971; Siems, 1973; Siems et al., 1974). Compared  
 1448 to other basalt-hosted aquifers, the Snake River Plain  
 1449 aquifer is one of the thickest basalt-hosted aquifers in  
 1450 the world (cf. Siems, 1973; Cheney and Farr, 1980;  
 1451 Cheney, 1981; Cheney, pers. comm.; Versey and  
 1452 Singh, 1982; Buckley and Oliver, 1990; Hooper,  
 1453 1997). The thinnest zones in the aquifer correspond  
 1454 to areas where the groundwater is warm and water  
 1455 chemistry indicates long residence time and input of  
 1456 geothermal fluids from depth (Smith et al., 2002).

1457 3. The thickest aquifer zones correspond to areas  
 1458 where the aquifer temperatures remain cool and most-  
 1459 ly isothermal to great depths with sharp inflections to  
 1460 the regional high geothermal gradient.

1461 4. Plumes of cold recharge water from local drain-  
 1462 ages are quickly warmed in some areas and form  
 1463 sharp incursions into warmer aquifer waters in other  
 1464 places.

### 38. Temperature logs—potential problems of interpretation

1465  
 1466  
 1467 Continental basaltic terrains present a unique  
 1468 problem for temperature logging. The extremely  
 1469 porous and permeable nature of the basalts allow  
 1470 easy circulation of fluids (both groundwater and air).  
 1471 In younger basalts, vigorous aquifers commonly  
 1472 form, dramatically affecting heat flow and shallow  
 1473 temperature distributions. In addition, barometric  
 1474 circulation of air to great depths often controls or  
 1475 influences the temperature of rocks above the water  
 1476 table. Because of the temperature effects of these  
 1477 fluids, basaltic terrains are not good candidates for  
 1478 assessment of long-term climatic temperature  
 1479 changes from borehole temperature logs. Also, ex-  
 1480 tremely deep wells are often required for determina-  
 1481 tion of accurate heat flow and regional geothermal  
 1482 gradients.

1483 **39. Discussion**

1484

1485 *39.1. Distinguishing individual layers within a basalt*  
1486 *sequence*

1487 Determining the depth and thickness of flows, flow  
1488 groups, and interbeds in a single borehole through a  
1489 basalt sequence is greatly simplified because of the  
1490 consistent and characteristic log signature of basalt  
1491 flow interiors. Flow interiors are the least fractured of  
1492 all basalt features, so they will have high acoustic  
1493 velocities; they are aquitards, so their neutron flux will  
1494 be very high; and they are dense and lack vesicles, so  
1495 their gamma–gamma counts on a density log will be  
1496 low. Dense, unfractured, and unaltered basalt is a  
1497 good electric insulator, so resistivity will be very high  
1498 for flow interiors. The best logs to identify flow  
1499 interiors are resistivity and velocity, both of which  
1500 alone may be sufficient in saturated and subaquifer  
1501 conditions (e.g., Fig. 8). In unsaturated conditions,  
1502 neutron logs can sometimes be sufficient to delineate  
1503 flow interiors (Siems, 1973; Siems et al., 1974),  
1504 though in some areas like the East Snake River Plain,  
1505 the neutron log needs to be supplemented by a natural  
1506 gamma or gamma–gamma log to avoid misinterpre-  
1507 tation (e.g., Fig. 6).

1508 Flow tops, flow bottoms, fracture zones, and  
1509 interbeds are not as easy to distinguish as flow  
1510 interiors, since these features commonly display var-  
1511 iable alteration, water content, fracturing, and density.  
1512 Fracture zones in basalt will slow velocity and might

affect neutron flux depending on the water or clay 1513  
content, but should not noticeably affect the gamma– 1514  
gamma counts on a density log because bulk density 1515  
is relatively unchanged unless large voids spaces are 1516  
present (e.g., collapsed lava tubes). In comparison, 1517  
the vesicular tops and bottoms of flows will be less 1518  
dense and are commonly fractured and oxidized, 1519  
resulting in decreased bulk density and magnetic 1520  
susceptibility and significantly degraded velocity 1521  
(e.g., Bücker et al., 1998). Flow tops and bottoms 1522  
are also preferred sites for alteration and are com- 1523  
monly the water-bearing zones in saturated condi- 1524  
tions, both of which will decrease neutron flux (e.g., 1525  
Cheney, 1981). Interbeds are less predictable. The 1526  
typical interbed has a signature of elevated natural 1527  
gamma counts, low velocity, low resistivity, low 1528  
neutron flux, and low bulk density. However, while 1529  
both velocity and neutron flux are almost always low 1530  
in an interbed, both natural gamma response and bulk 1531  
density can vary widely depending upon composition 1532  
and texture. 1533

1534 *39.2. Hydrogeological divisions within a basalt*  
1535 *sequence* 1536

1537 The hydrogeological divisions of a basalt flow 1538  
sequence can be determined with a minimum of either 1539  
a temperature or neutron log (see Table 2)—one of the 1540  
only instances where a single type of log can com- 1541  
pletely determine the variation in a basalt character- 1542  
istic for an entire flow sequence. 1543

t2.1 Table 2  
t2.2 Wireline analyses of hydrogeological zones in basalt flow sequences

t2.3	Log type	Natural gamma log	Neutron log	Gamma–gamma density log	Temperature log
t2.4	Unsaturated basalt	Low natural gamma counts in flow interiors, higher elsewhere	Highest neutron flux in flow interiors; moderate neutron flux at flow breaks and interbeds; average flux high	Low gamma flux in flow interiors, higher elsewhere	Positive temperature gradient
t2.5	Water-saturated basalt (basalt-hosted aquifer)	Uncorrected natural gamma counts attenuated by water, lower compared to unsaturated basalt	Lowest neutron flux in saturated interbeds, flow breaks and fracture zones; moderate to high flux in flow interiors; average flux low	Uncorrected gamma flux attenuated by water, lower compared to unsaturated basalt	Flat temperature gradient through saturation zone
t2.6	Subaquifer basalt	Generally low natural gamma counts, often indistinguishable from natural gamma response of basalt in the aquifer zone	Low to moderate neutron flux at flow breaks and interbeds; moderate flux in flow interiors; average flux moderate	Low gamma flux in unaltered flow interiors; lowest gamma flux when fractures and vesicles filled w/ alteration minerals	Positive lithostatic temperature gradient

1543 The temperature log can discern the three hydro-  
 1544 geological divisions because of the temperature differ-  
 1545 ences in porous basalt cooled by air and recharge  
 1546 water, porous basalt hosting the aquifer, and imper-  
 1547 meable altered basalt subject to the high regional  
 1548 geothermal heat gradient. To see the transition be-  
 1549 tween unsaturated and saturated conditions, the neu-  
 1550 tron log should be left uncorrected and the log trace  
 1551 should be presented on the same scale above and  
 1552 below the water table, like that for USGS-30 (Fig. 5)  
 1553 as opposed to the scale adjustments by Siems (1973)  
 1554 for Columbia River Plateau basalts (Fig. 4). All of the  
 1555 nuclear logs can distinguish the unsaturated zone/  
 1556 aquifer boundary because both neutron and gamma  
 1557 fluxes are attenuated by water. Only the neutron log,  
 1558 however, is sensitive to the transition from the satu-  
 1559 rated to the subaquifer alteration zone because of the  
 1560 contrast in average H content. Neither the natural  
 1561 gamma nor gamma–gamma density logs show suffi-  
 1562 cient contrast between the saturated and subaquifer  
 1563 alteration zones to distinguish this boundary.

1564 The combination of temperature logs and neutron  
 1565 logs is particularly powerful for mapping water-  
 1566 saturated zones in basalt. Supplementing these with  
 1567 velocity or resistivity logs to locate fracture zones,  
 1568 and fluid resistivity logs to locate changes in water  
 1569 chemistry can greatly refine knowledge of hydraulic  
 1570 conductivity within an aquifer. Flowmeters and fluid  
 1571 resistivity logs were not discussed in this paper,  
 1572 since these behave the same regardless of lithology,  
 1573 but it should be evident that their addition to an  
 1574 aquifer mapping program could greatly enhance the  
 1575 investigation.

1576  
 1577 *39.3. Stratigraphic correlation in a basalt sequence*

1578 There are three useful methods for stratigraphic  
 1579 correlations between several boreholes in a basalt  
 1580 sequence, each with different track records. First, a  
 1581 minimum combination of natural gamma, neutron,  
 1582 and gamma–gamma (density) logs should be suffi-  
 1583 cient to establish basic correlations between bore-  
 1584 holes, especially in flood basalts (e.g., Versey and  
 1585 Singh, 1982). When these conventional logs have  
 1586 produced questionable correlations, it is most often  
 1587 because too few tools were used, like natural gam-  
 1588 ma alone, or that individual features in a borehole  
 1589 were misidentified, as in the case of fracture zones

1590 infilled with sediments misidentified as sedimentary  
 1591 interbeds.

1592 Magnetic inclination is a very powerful tool for  
 1593 determining stratigraphy, though it is underutilized in  
 1594 continental basalts. The viability of the overall meth-  
 1595 od, however, has been amply demonstrated by the  
 1596 extensive paleomagnetic studies of cores collected  
 1597 from boreholes on the Snake River Plain (e.g., Cham-  
 1598 pion and Lanphere, 1997; Lanphere et al., 1994;  
 1599 Kuntz et al., 1980). Since magnetic polarity logging  
 1600 has been successful in the past in volcanic rocks (Scott  
 1601 and Olsen, 1985), the only impediment to using this  
 1602 method is the availability of magnetic wireline tools  
 1603 capable in and calibrated for basalt.

1604 Geochemical logging is a powerful tool for strati-  
 1605 graphic correlation (Anderson et al., 1990a,b). The  
 1606 end product of most geochemical logging methods is  
 1607 a qualitative or quantitative estimate of major and  
 1608 some trace element abundances. Natural gamma,  
 1609 gamma–gamma, natural gamma spectroscopy, in-  
 1610 duced-gamma spectroscopy, and neutron logs have  
 1611 all been used to estimate and correlate various ele-  
 1612 mental abundances. Several nuclear techniques used  
 1613 in combination should be adequate to correlate flows  
 1614 and interbeds between boreholes.

1615  
 1616 *39.4. Caveats of borehole geophysical logs in basalt*

1617 One common problem concerning data analysis in  
 1618 basalt sequences is that one tool alone, rather than a  
 1619 combination of tools, has been used to interpret  
 1620 breaks and internal stratigraphy. For example, natural  
 1621 gamma logs have been used extensively to discrim-  
 1622 inate flow architecture (e.g., Barraclough et al., 1976;  
 1623 Anderson and Lewis, 1989) and interbeds with ele-  
 1624 vated natural gamma counts (e.g., Versey and Singh,  
 1625 1982; Buckley and Oliver, 1990). Basalt flows,  
 1626 however, do not always show sufficient contrast in  
 1627 natural gamma counts to distinguish flows groups  
 1628 (e.g., Cheney, 1981), nor do interbeds always emit  
 1629 higher natural gamma flux (e.g., Quincy diatomite;  
 1630 Siems, 1973). Furthermore, the presence of a natural  
 1631 gamma peak may reflect sediment which has infilled  
 1632 cracks in the interior of a flow, or sediments sand-  
 1633 wiced between the former ceiling and floor of a  
 1634 collapsed lava tube. Natural gamma logs need to be  
 1635 interpreted in tandem with other tools, like gamma–  
 1636 gamma and/or neutron logs, which are also sensitive

t3.3	Log type	Natural gamma	Neutron	Gamma–gamma density	Resistivity <sup>a</sup>	Velocity <sup>b</sup>	Magnetic susceptibility	Magnetic polarity	Geochemical
t3.1	Table 3								
t3.2	Wireline analyses of basalt flow sequences								
t3.4	Physical basis of measurement	Natural gamma decay of K, Th, U	Scattering and capture of neutrons	Attenuation of active gamma flux by Compton scattering ( $\propto$ electron density)	Resistance to electric current	Ease of propagation of acoustic wave	Strength of induced magnetization	Direction of the remanent magnetization vector	A combination of multiple radiation sources plus detectors to measure total and spectral fluxes
t3.4	Utility for determining basalt stratigraphy	Can distinguish between flow groups. Can distinguish between basalt and interbeds	Can identify flow breaks or interbeds in the unsaturated zone, and fracture zones, flow breaks and/or interbeds below water table	Can distinguish between basalt and interbeds. Can be used to calculate bulk density. Can help identify collapse structures due to decreased density	Can distinguish between flows and flow breaks/interbeds, and between fractured and unfractured basalt	Can distinguish between flows and flow breaks/interbeds	Can distinguish between unaltered basalt and interbeds. Can distinguish between flow interiors and flow margins. Can identify oxidized basalt	Can identify polarity of remanence, help establish geochronology, help distinguish flow groups	Can determine the variation of several major element abundances, to distinguish between flows, flow groups, interbeds and alteration zones
t3.5	Limitations	Cannot discriminate between basalt and low K/U/Th interbeds, or between flow groups with low K/U/Th contrast	Cannot distinguish between flow breaks, fracture zones or interbeds; or between the effect of water vs. hydrous minerals on neutron flux	Presence of water will attenuate gamma flux	Cannot discriminate between flow breaks and fracture zones; or between conductivity due to water vs. conductivity due to hydrous minerals	Cannot discriminate between fracture zones, flow breaks and interbeds	Cannot discriminate oxidized basalt from other magnetic-mineral bearing rocks	Relatively insensitive to finer stratigraphic details	Level of detail can possibly obscure larger-scale features, elemental abundance determination only as good as the oxide-closure mode used
t3.6									
t3.7									
t3.8	<i>Sequence-scale features</i>								
t3.9	Unsaturated basalt	Natural gamma counts generally low in flows, usually higher in most sedimentary interbeds	Highest neutron flux in flow interiors; moderate neutron flux at flow breaks and interbeds	Low gamma flux in flow interiors, higher elsewhere	Highest possible resistivity in flow interiors if resistivity can be measured; lower at flow breaks and interbeds	High velocity, attenuated by fractures and flow breaks, if velocity can be measured	Dominated by ferrous magnetic minerals		

(continued on next page)

t3.10	Table 3 (continued)								
t3.11	Log type	Natural gamma	Neutron	Gamma–gamma density	Resistivity <sup>a</sup>	Velocity <sup>b</sup>	Magnetic susceptibility	Magnetic polarity	Geochemical
t3.12	<i>Sequence-scale features</i>								
t3.13	Water-saturated basalt (basalt-hosted aquifer)	Natural gamma counts always low: uncorrected gamma flux attenuated by water	Lowest neutron flux in saturated interbeds, flow breaks and fracture zones; moderate to high flux in flow interiors	Lower uncorrected gamma flux attenuated by water	High resistivity in flow interiors, lower resistivity at flow breaks	High velocity, attenuated by fractures and flow breaks when present	Potentially lower X from oxidation of ferrous oxides		
t3.14	Subaquifer basalt	Generally low, often indistinguishable from natural gamma response of basalt in the aquifer zone	Low to moderate neutron flux at flow breaks and interbeds; moderate flux in flow interiors	Low gamma flux in flow interiors without alteration; lowest gamma flux when fractures and vesicles filled w/ alteration minerals	Moderate to high resistivity in flow interiors, lower resistivity at flow breaks	Same or slightly higher velocity, attenuated by fractures and flow breaks when present	Potentially lower X from oxidation of ferrous oxides and growth of alteration minerals	Alteration may reset remanence	
t3.15	<i>Inter-flow features</i>								
t3.16	<i>Inter-flow features</i>								
t3.17	Flow tops and bottoms	Generally lower natural gamma counts than interbeds, higher than flow interiors	Moderate to low neutron flux	Moderate gamma flux, higher than flow interiors	Lower resistivity than flow interiors	Lower velocity than flow interior	Highest X at chilled margin (grain size effect) unless oxidized		
t3.18	Flow interiors	Lowest natural gamma counts	Highest neutron flux	Lowest gamma flux (highest density)	Highest possible resistivity	Highest possible velocity	High X		Can help correlate flows
t3.19	Clayey interbed	Highest natural gamma counts since most silts and clays have higher K than basalt	H in unsaturated clay will lower neutron flux compared to unsaturated basalt; saturated basalt may have lower neutron flux than a clayey aquiclude	Variable effect: gamma flux decreases with increasing clay content, positive density error introduced when hydrous minerals are present	Resistivity decrease due to conductive clay minerals	Low velocity	X decreases due to lower ferrous magnetic mineral content and increase in oxidation		Can help correlate interbeds

t3.20	Low-clay interbed	Natural gamma counts usually higher than basalt except in low-K rocks like limestone or diatomite	Neutron flux increases due to greater effective porosity	Gamma flux increases due to decrease in density	Resistivity decrease, especially if comparing the resistivity of flow interiors to interbeds	Low velocity	X decreases due to lower ferrous magnetic mineral content and increase in oxidation	Can help correlate interbeds
t3.21								
t3.22	<i>Intra-flow features</i>							
t3.23	Clay and/or zeolite alteration of basalt	Low natural gamma counts, slight increase compared to unaltered basalt	Lowered neutron flux (excess porosity error)	Low to moderate gamma flux	Lowered resistivity	Little or no increase in velocity compared to basalt Alteration may reset remanence	Lowered X	Attention may reset remanence
t3.24	Fracture zones	Variable: large void spaces decrease natural gamma counts; clayey minerals in fractures usually increase natural gamma counts	Low neutron flux in saturated conditions; high to moderate flux in unsaturated conditions, lower if hydrous minerals present	Apparent density drop, gamma flux increases	Usually low resistivity, though variable depending on content and distribution of voids and infilled clays	Usually lower than most flow margins	Variable	Remanence directions may be unreliable in basalt rubble or in basalt disturbed by fracturing
t3.25	Collapse structures (lava tubes, etc.)	In general, very low natural gamma counts, lower than most flows		Higher gamma flux			Variable	
t3.26	Scoria, cinders	Low natural gamma counts		Moderate to high gamma flux			Higher X in unoxidized scoria; lowered X typical of hematite in cinders and oxidized scoria	

t3.27 <sup>a</sup> Usually used in saturated conditions only, excludes induction logs which are not suitable for basalt.

t3.28 <sup>b</sup> Usually used in saturated conditions only.

1637 to flow architecture. Details on tool combinations that  
1638 are advisable for wireline logging are presented in  
1639 [Tables 3 and 4](#), which summarize the physical prop-

t4.1	Table 4		
t4.2	Effective wireline tools in basalt		
t4.3	Basalt property or characteristic	Effective tools and tool combinations	
t4.4	<i>Mineral and elemental composition</i>		
	K, Th, U	Natural gamma, natural gamma spectroscopy, geochemical	
t4.5	Magnetic minerals	Magnetic susceptibility	
t4.6	Ca, Cl, Fe, H, S, and Si	Neutron-spectral gamma—capture mode	
t4.7	Ca, C, Fe, O, S, and Si	Neutron-spectral gamma—inelastic mode	
t4.8	K, Si, Ca, Fe, S, Ti, Al, U, Th, Gd, Mg	Natural gamma, neutron, magnetic susceptibility, natural spectral gamma, neutron—spectral gamma, gamma—gamma density w/PEF, geochemical	
t4.9			
t4.10			
t4.11	<i>Stratigraphic features</i>		
	Location and thickness of flow interiors	Any combination of very high resistivity <sup>a</sup> , high velocity <sup>b</sup> , high neutron flux, low gamma flux on gamma—gamma density log	
t4.12	Correlation of basalts flows between boreholes	Magnetic polarity and/or geochemical (including natural gamma)	
t4.13	Paleomagnetic geochronology	Combination of magnetic polarity, magnetic susceptibility, gyroscope	
t4.14	Aquifer thickness	Combination of low neutron + low/no temperature gradient	
t4.15			
t4.16			
t4.17	<i>Intra-flow features</i>		
	Fracture zones with no sediment infilling	Combinations of attenuated or no velocity <sup>b</sup> , extremely low natural gamma counts, high gamma flux on gamma—gamma density log, large variable caliper, low neutron flux in saturated conditions	
t4.18	Fracture zones with sediment infilling	Combinations of attenuated or no velocity <sup>b</sup> , large variable caliper, low neutron flux in saturated conditions, decreased gamma flux on gamma—gamma density log	
t4.19	Hydrous alteration minerals	Combination of low neutron + elevated natural gamma, or of low neutron + increased gamma flux on gamma—gamma density log	
t4.20	Collapse structures	Combination of extremely low natural gamma counts, high gamma flux on gamma—gamma density log, large caliper measurements	
t4.21			
t4.22		<sup>a</sup> Usually used in saturated conditions only, induction logs not recommended.	
t4.23		<sup>b</sup> Usually used in saturated conditions only.	

erties measured by most of the tools discussed and  
how these properties vary stratigraphically in conti-  
nental basalt sequences.

Porosity is probably the most difficult physical parameter to determine in basalt. Every study reviewed here that has used neutron logs in basalt has noted a positive error in saturated porosity introduced by hydrous clay or zeolite minerals. In resistivity logging, these hydrous minerals also introduce a positive error in effective porosity, even when using a highly modified basalt-specific Archie's Law. When hydrous minerals are present, their contribution to neutron and resistivity logs cannot be quantitatively determined unless corrected for using a method like that developed by [Broglia and Ellis \(1990\)](#). For this reason, traditional wireline logs in basalt should be expressed in terms of the physical parameters which are directly measured by each tool, not in terms of calculated or inferred parameters like density or porosity. Reporting tool response in terms of uncorrected physical parameters is also useful for identifying the hydrogeological divisions within a basalt flow sequence (e.g., saturated vs. unsaturated), with the caveat that the saturated and unsaturated response of most tools may be irreconcilable if the tools have not been carefully calibrated for both environments.

## 40. Conclusion

Interpreting borehole geophysical logs from basalt requires a fundamental understanding of both the tool and basalt volcanology. Data should be measured in terms of what each wireline tool actually measures, and not in terms of the physical properties a tool is assumed to measure in the sedimentary environment. [Table 3](#) summarizes the tools discussed in this paper, the actual property measured by each tool and the stratigraphic features it is sensitive to in a continental basalt sequence. We have found that in basalt provinces with substantial unsaturated zones, it is often useful not to correct for the presence of fluid in the borehole, but rather to use the uncorrected logs to help map aquifers, and to identify zone of higher hydraulic conductivity within aquifers. Determining porosity is perhaps the most problematic issue in applying borehole geophysical methods in basalt, and in general, neutron and resistivity logs should be used cautiously

1685 for this purpose because of the difficulty in identifying  
1686 and compensating for the error introduced by hydrous  
1687 minerals like clays and zeolites.

1688 The success of a borehole geophysical investigation  
1689 to determine stratigraphy will depend on selecting an  
1690 appropriate combination of tools to measure properties  
1691 appropriate for basalt. Geochemical and magnetic  
1692 polarity logging are two of the most powerful methods  
1693 for determining stratigraphic features in basalt sequen-  
1694 ces, though less common than using several standard  
1695 and easily available tools in combination. Determining  
1696 a comprehensive stratigraphic sequence in basalt can  
1697 be done with a minimum of five commonly available  
1698 tools: natural gamma, neutron, velocity, resistivity, and  
1699 gamma–gamma density. Neutron, gamma–gamma  
1700 density, resistivity, and velocity tools will locate the  
1701 flow interiors. The intelligent comparison of natural  
1702 gamma, neutron, velocity, and gamma–gamma densi-  
1703 ty logs should identify fracture zones, flow tops and  
1704 bottoms, and most interbeds. Natural gamma, gam-  
1705 ma–gamma density, and caliper logs should suffice to  
1706 identify any collapsed structures still harboring void  
1707 spaces. Upgrading to a natural gamma spectrum tool  
1708 and adding magnetic susceptibility will enhance and  
1709 refine the details of the stratigraphic column.

## 1710 Acknowledgements

1711 This research was funded by a grant from the  
1712 Inland Northwest Research Association, and we  
1713 sincerely thank them for their support. We also wish  
1714 to thank Phil Nelson, Steve Anderson, and Linda  
1715 Davis of the USGS for fielding our many requests for  
1716 information and log data; and Duane Champion and  
1717 Ted Herman at the USGS for insights and access to  
1718 their magnetic properties datasets for the Snake River  
1719 Plain. We would like to thank Colin Cheney of the  
1720 British Geological Survey, Fred Paillet of the USGS  
1721 (now at U. of Maine), and David Goldberg of the  
1722 Lamont-Doherty Earth Observatory/Columbia Uni-  
1723 versity for answering the questions we had for them.  
1724 We wish to acknowledge Fred Paillet, Peter Fullagar,  
1725 and Carl Koizumi for their patience and understanding  
1726 in the face of our disorganization in submitting this  
1727 study, and to thank Peter Fullagar and Carl Koizumi  
1728 for their thoughtful reviews which greatly improved  
1729 this paper. Last but in no way least, we wish to thank

Cheryl Whitaker of the Hydrogeological Data Repo- 1730  
sitory at the INEEL for all her help in accessing and 1731  
making sense of over 50 years worth of geophysical 1732  
log data collected on the Eastern Snake River Plain— 1733  
we could not have done this study without her. 1734

## References 1735

- Anderson, S.R., Bartholomay, R.C., 1995. Use of natural-gamma 1736  
logs and cores for determining stratigraphic relations of basalt 1737  
and sediment at the Radioactive Waste Management Complex, 1738  
Idaho National Engineering Laboratory, Idaho. *J. Idaho Acad.* 1739  
*Sci.* 31 (1), 1–10. 1740
- Anderson, S.R., Lewis, B.D., 1989. Stratigraphy of the Unsaturated 1741  
Zone at the Radioactive Waste Management Complex. Idaho 1742  
National Engineering Laboratory, Idaho. U.S. Geol. Survey 1743  
Water-Resources Investigations Report 89-4065. 54 pp. 1744
- Anderson, R.N., Honnorez, J., Becker, K., Adamson, A.C., Alt, 1745  
J.C., Emmermann, R., Kempton, P.D., Kinoshita, H., Laverne, 1746  
C., Mattl, M.J., Newmark, R.L., 1982. DSDP Hole 504B, the 1747  
reference section over 1 km through layer 2 of the oceanic crust. 1748  
*Nature* 300, 589–594. 1749
- Anderson, R.N., Dove, R.E., Preston, E., 1990a. Geochemical well 1750  
logs: calibration and lithostratigraphy in basaltic, granitic and 1751  
metamorphic rocks. In: Hurst, A., Lovell, M.A., Morton, A.C. 1752  
(Eds.), *Geological Applications of Wireline Logs*. Geol. Soc. 1753  
London Spec. Publ., vol. 48, pp. 177–194. 1754
- Anderson, R.N., Alt, J.C., Malpas, J., Lovell, M.A., Harvey, P.K., 1755  
Pratson, E.L., 1990b. Geochemical well logging in basalts: the 1756  
Palisades Sill and the Oceanic Crust of Hole 504B. *J. Geophys.* 1757  
*Res.* 95, 9265–9292. 1758
- Bailey, E.H., Irwin, W.P., Jones, D.L., 1964. Franciscan and related 1759  
rocks, and their significance in the geology of western Califor- 1760  
nia. *Calif. Div. Mines Geol. Bull.*, vol. 183. 177 pp. 1761
- Barraclough, J.T., Robertson, J.B., Janzer, V.J., 1976. Hydrology of 1762  
the Solid Waste Burial Ground, as related to the potential mi- 1763  
gration of radionuclides. Idaho National Engineering Labora- 1764  
tory. U.S. Geol. Survey Open File Report 76-471. 184 pp. 1765
- Bartolino, J.R., Niswonger, R.G., 1999. Numerical Simulation Of 1766  
Vertical Ground-Water Flux of the Rio Grande from Ground- 1767  
Water Temperature Profiles. Central New Mexico. U.S. Geol. 1768  
Survey, Water-Resources Investigations Report 99-4212. 45 pp. 1769
- Bates, D.L., 1999. The in situ chemical fractionation of an eastern 1770  
Snake River Plain basalt flow: implications for heterogeneous 1771  
chemical interaction with groundwater contaminants. Master's 1772  
Thesis. Idaho State University, Pocatello, Idaho. 146 pp. 1773
- Becker, K., Von Herzen, R.P., Francis, T.J.G., Anderson, R.N., 1774  
Honnorez, J., Adamson, A.C., Alt, J.C., Emmermann, R., 1775  
Kempton, P.D., Kinoshita, H., Laverne, C., Mattl, M.J., New- 1776  
mark, R.L., 1982. In situ electrical resistivity and bulk porosity 1777  
of the oceanic crust Costa Rica Rift. *Nature* 300, 594–598. 1778
- Becker, K., Sakai, H., Adamson, A.C., Alexandrovich, J., Alt, J.C., 1779  
Anderson, R.N., Bodeau, D., Gable, R., Herzig, P.M., Houghton, 1780  
S., Ishizuka, H., Kawahata, H., Kinoshita, H., Langseth, M.G., 1781  
Lovell, M.A., Malpas, J., Masuda, H., Merrill, R.B., Morin, 1782

- 1783 R.H., Mottl, M.J., Pariso, J.E., Pezard, P., Phillips, J., Sparks, J.,  
 1784 Uhlig, S., 1989. Drilling deep into young oceanic crust, Hole  
 1785 504B, Costa Rica Rift. *Rev. Geophys.* 27 (1), 79–102.
- 1786 Beeson, M.H., Clague, D.A., Lockwood, J.P., 1996. Origin and  
 1787 depositional environment of clastic deposits in the Hilo Drill  
 1788 Hole, Hawaii. *J. Geophys. Res.* 101, 11617–11629.
- 1789 Belknap, W.B., Dewan, J.T., Kirkpatrick, C.V., Mott, W.E., Pera-  
 1790 son, A.J., Rabson, W.R., 1960. API Calibration Facility for  
 1791 Nuclear Logs. American Petroleum Institute Drilling Production,  
 1792 p. 289.
- 1793 Blackwell, D.D., 1989. Regional implications of heat flow of the  
 1794 Snake River Plain, northwestern United States. *Tectonophysics*  
 1795 164, 323–343.
- 1796 Blackwell, D.D., Steele, J.L., 1992. Geothermal map of North  
 1797 America. DNAG Continent-Scale Map-006. *Geol. Soc. of*  
 1798 *America. Decade of North American Geology series.*
- 1799 Blackwell, D.D., Murphey, C.S., Steele, J.L., 1982. Heat flow and  
 1800 geophysical log analysis for OMF-7A geothermal test well,  
 1801 Mount Hood, Oregon. In: Priest, G.R., Vogt, B.F. (Eds.), *Geol-*  
 1802 *ogy and Geothermal Resources of the Mount Hood area. Ore-*  
 1803 *gon, State of Oregon Department of Geology and Mineral*  
 1804 *Industries Special Paper, vol. 14, pp. 47–56.*
- 1805 Blair, J.J., 2002. Sedimentology and Stratigraphy of Sediments of  
 1806 the Big Lost Trough Subsurface from Selected Coreholes at the  
 1807 Idaho National Engineering and Environmental Laboratory, Ida-  
 1808 ho. Master's Thesis. Idaho State University, Pocatello, Idaho.  
 1809 148 pp.
- 1810 Brewer, K., Sakai, H., Adamson, A.C., Alexandrovich, J., Alt, J.C.,  
 1811 Anderson, R.N., Bideau, D., Gable, R., Herzig, P.M., Houghton,  
 1812 S., Ishizuka, H., Kawahata, H., Langseth, M.G., Lovell, M.A.,  
 1813 Malpas, J., Masuda, H., Merrill, R.B., Morin, R.H., Mottl, M.J.,  
 1814 Pariso, J.E., Pezard, P., Phillips, J., Sparks, J., Uhlig, S., 1989.  
 1815 Drilling deep into young ocean crust, Hole 504B, Costa Rica  
 1816 Rift. *Rev. Geophys.* 27 (1), 79–102.
- 1817 Brewer, T.S., Lovell, M.A., Harvey, P.K., Pelling, R., Atkin, B.P.,  
 1818 Adamson, A., 1990. Preliminary geochemical results from  
 1819 DSDP/ODP Hole 504B: a comparison of core and log data.  
 1820 In: Hurst, A., Lovell, M.A., Morton, A.C. (Eds.), *Geological*  
 1821 *Applications of Wireline Logs. Geol. Soc. London Spec. Publ.,*  
 1822 *vol. 48, pp. 195–202.*
- 1823 Brewer, T.S., Harvey, P.K., Lovell, M.A., Haggas, S., Williamson,  
 1824 G., Pezard, P., 1998. Ocean floor volcanism: constraints from  
 1825 the integration of core and downhole logging measurements.  
 1826 In: Harvey, P.K., Lovell, M.A. (Eds.), *Core-Log Integration.*  
 1827 *Geol. Soc. London Spec. Publ., vol. 136, pp. 341–362.*
- 1828 Broglia, C., Ellis, D., 1990. Effect of alteration, formation absorp-  
 1829 tion, and standoff on the response of the thermal neutron porosity  
 1830 log in Gabbros and Basalts: examples from Deep Sea Drilling  
 1831 Project-Ocean Drilling Program Sites. *J. Geophys. Res.* 95,  
 1832 9171–9188.
- 1833 Brott, C.A., Blackwell, D.D., Ziagos, J.P., 1981. Thermal and tec-  
 1834 tonic implications of heat flow in the eastern Snake River Plain,  
 1835 Idaho. *J. Geophys. Res.* 86, 11709–11734.
- 1836 Brune, J.N., Henyey, T.L., Roy, R.F., 1969. Heat flow, stress, and  
 1837 rate of slip along the San Andreas fault, California. *J. Geophys.*  
 1838 *Res.* 74, 3821–3827.
- 1839 Bucker, C.J., Cashman, K.V., Planke, S., 1998. Physical and mag-  
 netic characterization of aa and pahoehoe flows: Hole 990A. In:  
 Larsen, H.C., Duncan, R.A., Allan, J.F., Brooks, K. (Eds.), *Proc.*  
 ODP, Sci. Results, vol. 163. [http://www-odp.tamu.edu/publications/163\\_SR/chap\\_05/chap\\_05.htm](http://www-odp.tamu.edu/publications/163_SR/chap_05/chap_05.htm) (accessed 28 Aug. 2001).
- Buckley, D.K., Oliver, D., 1990. Geophysical logging of water  
 exploration boreholes in the Deccan Traps, Central India. In:  
 Hurst, A., Lovell, M.A., Morton, A.C. (Eds.), *Geological Ap-*  
 plications of Wireline Logs. *Geol. Soc. London Spec. Publ.,*  
 vol. 48, pp. 153–161.
- Butler, R.F., 1992. *Paleomagnetism Blackwell Scientific Publica-*  
 tions, Boston. 319 pp.
- Champion, D.E., Lanphere, M.A., 1997. Age and paleomagnetism  
 of basaltic lava flows in corehole ANL-OBS-AQ-014 at Ar-  
 gonne National Laboratory-West. Idaho National Engineering  
 and Environmental Laboratory. U.S. Geol. Survey Open File  
 Report 97-700. 34 pp.
- Chase, G.H., Teasdale, W.E., Ralston, D.A., Jenson, R.G., 1964.  
 Completion report for observation wells 1 through 49, 51, 54,  
 55, 56, 80, and 81 at the National Reactor Testing Station,  
 Idaho. United States Atomic Energy Commission Report  
 IDO-22045-USGS.
- Cheney, C.S., 1981. Hydrogeological investigations into the Strom-  
 berg Basalts of the Lephpe/Dibete area. Republic of Botswana  
 Dept. of Geol. Survey Report GS10/13. Lobatse.
- Cheney, C.S., Farr, J.L., 1980. Results of the borehole geophysical  
 logging, physical properties core analysis and aquifer testing in  
 the Serowe study block. Republic of Botswana Dept. of Geol.  
 Survey GS10 Technical Note No. 7. Lobatse.
- Clark, D.A., Emerson, D.W., 1991. Notes on rock magnetization  
 characteristics in applied geophysical studies. *Explor. Geophys.*  
 22 (3), 547–555.
- Crosby, J.W., Anderson, J.V., 1971. Some applications of geophys-  
 ical well logging to basalt hydrology. *Ground Water* 9 (5), 12–20.
- Dean, J.A., 1995. *Analytical Chemistry Handbook.* McGraw-Hill,  
 NYC. 1168 pp.
- Doherty, D.J., 1979. Drilling data from exploration well 2-2A, NW  
 1/4, Sec. 15, T. 5 N., R. 31 E. Idaho National Engineering  
 Laboratory, Butte County, Idaho. United State Geological Sur-  
 vey Open-File Report 79-851. 1 sheet.
- Draxler, J.K., 1990. Geochemical Logging Tool (GLT)—Logaus-  
 wertung in kristallinen Gesteinen. *Zentralbl. Geol. Palaeontol.*  
 Teil 1, Allgemeine, Angew. 8, 1003–1019.
- Dunlop, D.J., Ozdemir, O., 1997. *Rock Magnetism.* Cambridge  
 Univ. Press. 573 pp.
- Ehlers, E.G., Blatt, H., 1982. *Petrology: Igneous, Sedimentary and*  
*Metamorphic.* W.H. Freeman & Co., San Francisco. 732 pp.
- Fukuma, K., 1998. 23. Origin and applications of whole-core mag-  
 netic susceptibility of sediments and volcanic rocks from  
 Leg152. In: Saunders, A.D., Larsen, H.C., Wise Jr., S.W.  
 (Eds.), *Proceedings of the Ocean Drilling Program. Scientific*  
*Results, vol. 152, pp. 271–280.*
- Goldberg, D., 1997. The role of downhole measurements in marine  
 geophysics. *Rev. Geophys.* 35, 315–342.
- Greeley, R., 1982a. The Snake River Plain, Idaho: representative of  
 a new category of volcanism. *J. Geophys. Res.* 87, 2705–2712.
- Greeley, R., 1982b. The style of Basaltic Volcanism in the Eastern  
 Snake River Plain, Idaho. In: Bonnicksen, B., Breckenridge,

- 1897 R.M. (Eds.), Cenozoic Geology of Idaho. Idaho Bur. Mines  
1898 Geol. Bull., vol. 26, pp. 407–421.
- 1899 Greeley, R., King, J.S., 1975. Geologic field guide to the Quater-  
1900 nary volcanics of the south-central Snake River Plain, Idaho.  
1901 Idaho Bur. Mines Geol. Pam., vol. 160. 49 pp.
- 1902 Haggas, S.L., Brewer, T.S., Harvey, P.K., 2002. Architecture of the  
1903 volcanic layer from the Costa Rica Rift, constraints from core-  
1904 log integration. *J. Geophys. Res.* 107 (B2), 1–14 (10.1029/  
1905 2001JB000147, ECV 2).
- 1906 Harris, R.N., Chapman, D.S., 1997. Borehole temperatures and a  
1907 baseline for 20th-century global warming estimates. *Science*  
1908 275, 1618–1621.
- 1909 Hawaii Scientific Drilling Project, 1993. [http://expet.gps.caltech.edu/Hawaii\\_project.html](http://expet.gps.caltech.edu/Hawaii_project.html) (accessed January 28, 2001).
- 1910 Herron, M.M., Herron, S.L., 1990. Geological applications of geo-  
1912 chemical well logging. In: Hurst, A., Lovell, M.A., Morton,  
1913 A.C. (Eds.), *Geological Applications of Wireline Logs*. Geol.  
1914 Soc. London Spec. Publ., vol. 48, pp. 165–175.
- 1915 Hertzog, R., Soran, P., Schweitzer, J., 1986. Applications of cross  
1916 section data for nuclear geochemical well logging. *J. Radiat.*  
1917 *Effects* 94, 49–52.
- 1918 Hertzog, R., Colson, L., Seeman, B., O'Brien, M., Scott, H.,  
1919 McKeon, D., Wraight, P., Grau, J., Schweitzer, J., Herron, M.,  
1920 1987. Geochemical logging with spectrometry tools. SPE Paper  
1921 16792, *Transactions Vol. 9*, Formation Evaluation and Reser-  
1922 voir Geology: Soc. of Petroleum Engineers, 447–460.
- 1923 Hertzog, R., Ellis, D., Grau, J., Schweitzer, J., 1988. Elemental  
1924 concentrations from gamma ray spectroscopic logs. *Nucl. Geo-*  
1925 *phys.* 2, 175–182.
- 1926 Hooper, P.R., 1997. The Columbia River Flood Basalt Province:  
1927 current status. In: Mahoney, J.J., Coffin, M.F. (Eds.), *Large*  
1928 *Igneous Provinces: Continental, Oceanic, and Planetary Flood*  
1929 *Volcanism*. Am. Geophys. Union Monogr., vol. 100, pp. 1–27.
- 1930 Hughes, S.S., Smith, R.P., Hackett, W.R., Anderson, S.R., 1999.  
1931 Mafic volcanism and environmental geology of the Eastern  
1932 Snake River Plain, Idaho. In: Hughes, S.S., Thackray, G.D.  
1933 (Eds.), *Guidebook to the Geology of Eastern Idaho*: Idaho Mu-  
1934 seum of Natural History, pp. 143–168.
- 1935 Hughes, S.S., McCurry, M., Geist, D.J., 2002. Geochemical corre-  
1936 lations and implications for the magmatic evolution of basalt  
1937 flow groups at the Idaho National Engineering and Environmen-  
1938 tal Laboratory. In: Link, P.K., Mink, L.L. (Eds.), *Geology, Hydro-*  
1939 *geology, and Environmental Remediation*, Idaho National  
1940 Engineering and Environmental Laboratory, Eastern Snake River  
1941 Plain, Idaho. Geol. Soc. Am. Spec. Pap., vol. 353, pp. 151–174.
- 1942 International Continental Drilling Program/GeoForschungsZen-  
1943 trum-Potsdam, 1999. Hawaii Scientific Drilling Project data. Ar-  
1944 chived at: [http://icdp.gfz-potsdam.de/html/hawaii/data\\_pub.html](http://icdp.gfz-potsdam.de/html/hawaii/data_pub.html)  
1945 (accessed 24 Feb. 2001).
- 1946 Keys, W.S., 1990. Borehole geophysics applied to ground-water  
1947 investigations: techniques of water-resources investigations of  
1948 the U.S. Geol. Survey, Bk. 2, Chap. E2. 150 pp.
- 1949 Keys, W.S., MacCary, L.M., 1971. Application of borehole geo-  
1950 physics to water-resources investigations: U.S. Geological Sur-  
1951 vey Techniques of Water-Resources Investigations, Bk. 2, Chap.  
1952 El. 126 pp.
- 1953 Knutson, C.F., Sullivan, W.H., Dooley, K.J., 1994. Geotechnical  
logging evaluation of the Eastern Snake River Plain Basalts. Soc. of Prof. Well Log Analysts 34th Annual Logging Symposium, 1–17.
- Kuehn, S.C., 1995. The Olympic-Wallowa Lineament, Hite Fault System, and Columbia River Basalt Group Stratigraphy in northeast Umatilla County. Oregon, Master's Thesis. Washington State University, Pullman, Washington, [http://www.wsu.edu:8080/~sckuehn/mstthesis/appendix\\_d.html](http://www.wsu.edu:8080/~sckuehn/mstthesis/appendix_d.html) (accessed September 16, 2002).
- Kuntz, M.A., Dalrymple, G.B., Champion, D.E., Doherty, D.J., 1980. Petrography, age, and paleomagnetism of volcanic rocks at the Radioactive Waste Management Complex. Idaho National Engineering Laboratory, Idaho, with an evaluation of potential volcanic hazards. U.S. Geological Survey Open-File Report 80-388. 63 pp.
- Lachenbruch, A.H., Sass, J.H., 1980. Heat flow and energetics of the San Andreas fault zone. *J. Geophys. Res.* 85, 6185–6222.
- Lamont-Doherty Earth Observatory, 2001. Geochemical Tool (GLT). Ocean Drilling Program Logging Manual. <http://www.ideo.columbia.edu/BRG/ODP/LOGGING/TOOLS/geochem.html> (accessed April 16, 2002).
- Lanphere, M.A., Kuntz, M.A., Champion, D.E., 1994. Petrology, age, and paleomagnetism of basaltic lava flows in coreholes at Test Area North (TAN). Idaho National Engineering Laboratory. U. S. Geol. Survey Open File Report 94-686. 49 pp.
- Last, G.V., Horton, D.G., 2000. Review of Geophysical Characterization Methods Used at the Hanford Site, PNNL-13149. Pacific Northwest National Laboratory, Richland, WA. 113 pp.
- Lovell, M.A., Pezard, P.A., 1990. Electrical properties of basalts from DSDP Hole 504B: a key to the evaluation of pore space morphology. In: Hurst, A., Lovell, M.A., Morton, A.C. (Eds.), *Geological Applications of Wireline Logs*. Geol. Soc. London Spec. Publ., vol. 48, pp. 339–345.
- Macdonald, G.A., 1972. *Volcanoes* Prentice-Hall. Englewood Cliffs, NJ. 510 pp.
- Majorowicz, J.A., Safanda, J., Harris, R.N., Skinner, W.R., 1999. Large ground surface temperature changes of the last three centuries inferred from borehole temperatures in the Southern Canadian Prairies, Saskatchewan. *Global Planet. Change* 20, 227–241.
- Morin, R.H., Barrash, W., Paillet, F.L., Taylor, T.A., 1993. Geophysical logging studies in the Snake River Plain Aquifer at the Idaho National Engineering Laboratory—Wells 44, 45, and 46. U.S. Geol. Survey Water-Resources Investigations Report 92-4184. 44 pp.
- Morse, L.H., McCurry, M., 1997. Possible correlations between basalt alteration and the effective base of the Snake River Plain Aquifer at the Idaho National Engineering and Environmental Laboratory. Proceedings of the 32nd Symposium on Engineering Geology and Geotechnical Engineering, held at Boise, Idaho, March 26–28, 1997, 1–13.
- Morse, L.H., McCurry, M., 2002. Genesis of alteration of Quaternary basalts within a portion of the eastern Snake River Plain aquifer. In: Link, P.K., Mink, L.L. (Eds.), *Geology, Hydrogeology, and Environmental Remediation*, Idaho National Engineering and Environmental Laboratory, Eastern Snake River Plain, Idaho. Geol. Soc. Am. Spec. Pap., vol. 353, pp. 213–224.

- 2011 Nelson, P., 1993. Magnetic susceptibility logs from sedimentary  
2012 and volcanic environments. Soc. of Prof. Well Log Analysts  
2013 34th Annual Logging Symposium, V1-V15. 2053
- 2014 Pezard, P.A., 1990. Electrical properties of mid-ocean ridge basalt  
2015 and implications for the structure of the upper oceanic crust in  
2016 Hole 504B. *J. Geophys. Res.* 95, 9237-9266. 2054
- 2017 Pollack, H.N., Huang, S., Shen, P.-Y., 1998. Climate change record  
2018 in subsurface temperatures: a global perspective. *Science* 282,  
2019 279-281. 2055
- 2020 Priest, G.R., Beeson, M.H., Gannett, M.W., Berri, D.A., 1982. 2056
- 2021 Geology, geochemistry, and geothermal resources of the Old  
2022 Maid Flat area, Oregon. In: Priest, G.R., Vogt, B.F. (Eds.),  
2023 Geology and Geothermal Resources of the Mount Hood Area,  
2024 Oregon. State Oreg. Dept. Geol. Miner. Ind. Spec. Pap., vol. 14,  
2025 pp. 16-30. 2057
- 2026 Salisbury, M.H., Scott, J.H., Auroux, C., Becker, K., Bosum, W.,  
2027 Broglia, C., Carlson, R., Fisher, A., Gieskes, J., Holmes, M.A.,  
2028 Hoskins, H., Legrand, J., Moos, D., Rio, D., Stephen, R.A.,  
2029 Wilkens, R., 1986. Site 418: Bermuda Rise. Proc., Init. Repts.  
2030 (Pt. A), ODP 102, 95-149. 2058
- 2031 Schlumberger Wireline and Testing, 1989. Log Interpretation Prin-  
2032 ciples/Applications Sugarland, Texas. 251 pp. 2059
- 2033 Scott, J.H., Olsen, G.G., 1985. A three-component borehole mag-  
2034 netometer probe for mineral investigations and geologic re-  
2035 search. Soc. Prof. Well Log Analysts 26th Annual Logging  
2036 Symposium, vol. I, pp. E1-E16. 2060
- 2037 Scott, J.H., Zablocki, C.J., Clayton, G.H., 1979. Geophysical  
2038 well-logging data from exploratory Well 2-2A, NW 1/4 Sec.  
2039 15, T. 5 N., R. 31 E. Idaho National Engineering Laboratory,  
2040 Butte County, Idaho, U.S. Geol. Survey Open File Report  
2041 79-1460. 1 sheet. 2061
- 2042 Scott, J.H., Seeley, R.L., Barth, J.J., 1981. A magnetic susceptibility  
2043 well-logging system for mineral exploration. Soc. Prof. Well  
2044 Log Analysts 22nd Annual Logging Symposium, vol. II,  
2045 pp. CC1-CC21. 2062
- 2046 Scott, J.H., Daniels, J.J., Reynolds, R.L., Seeley, R.L., 1983. Mag-  
2047 netic-susceptibility logging in sedimentary uranium environ-  
2048 ments. *Log Anal.* 24 (2), 16-21. 2063
- 2049 Sharp, R.P., 1976. Field Guide Southern California (Rev. Ed.).  
2050 Kendall/Hunt Publishing, Dubuque, IA. 208 pp. 2064
- 2051 Siems, B.A., 1973. Surface to subsurface correlation of Columbia  
2052 River Basalt using geophysical data, in parts of Adams and  
Franklin Counties, Washington. Wash. State Univ. Coll. Eng.  
Bull. 331, 1-65. 2065
- Siems, B.A., Bush, J.H., Crosby, J.W., 1974. TiO<sub>2</sub> and geophysical  
logging criteria for Yakima Basalt correlation, Columbia Pla-  
teau. *Geol. Soc. Am. Bull.* 85, 1061-1068. 2066
- Skinner, W.R., Majorowicz, J.A., 1999. Regional climatic warming  
and associated twentieth century land-cover changes in north-  
western North America. *Clim. Res.* 12, 39-52. 2067
- Smith, R.P., Blackwell, D.D., McLing, T.L., 2002. Ground water  
flow, aquifer geometry, and geothermal interactions inferred  
from temperature distribution: Snake River Plain aquifer,  
south-eastern Idaho, Paper No. 42-5. *Geol. Soc. Am. Ann.  
Meet., Abstr. Progr.* 34 (6), 96. 2068
- Stolper, E.M., DePaolo, D.J., Thomas, D.M., 1996. Introduction of  
special section: Hawaii Scientific Drilling Project. *J. Geophys.  
Res.* 101, 11593-11598. 2069
- Swanberg, C.A., Walkey, W.C., Combs, J., 1988. Core hole drilling  
and the "rain curtain" phenomenon at Newberry volcano, Ore-  
gon. *J. Geophys. Res.* 93, 10163-10173. 2070
- Versey, H.R., Singh, B.K., 1982. Groundwater in the Deccan basalts  
of the Betwa basin, India. *J. Hydrol.* 58, 276-306. 2071
- Walker, G.P.L., 1972. Compound and simple lava flows and flood  
basalts. *Bull. Volcanol.* 36, 579-590. 2072
- Welhan, J.A., Johannesen, C.M., Reeves, K.S., Clemo, T.M., Glo-  
ver, J.A., Bosworth, K.W., 2002. Morphology of inflated pahoehoe  
lavas and spatial architecture of their porous and permeable  
zones, eastern Snake River Plain, Idaho. In: Link, P.K., Mink,  
L.L. (Eds.), *Geology, Hydrogeology, and Environmental Reme-  
diation, Idaho National Engineering and Environmental Labo-  
ratory, Eastern Snake River Plain, Idaho. Geol. Soc. Am. Spec.  
Pap., vol. 353, pp. 135-150.* 2073
- Wetmore, P.L., 1998. An assessment of physical volcanology and  
tectonics of the central eastern Snake River Plain based on the  
correlation of subsurface basalts at and near the Idaho National  
Engineering and Environmental Laboratory, Idaho, Master's  
Thesis. Idaho State University, Pocatello, Idaho, 118 pp. 2074
- Williams, C.F., Anderson, R.N., 1990. Thermophysical properties  
of the Earth's crust: in situ measurements from Continental and  
Ocean Drilling. *J. Geophys. Res.* 95, 9209-9236. 2075
- Ziagos, J.P., Blackwell, D.D., 1981. A model for the effect of  
horizontal fluid flow in a thin aquifer on temperature-depth  
profiles. *Trans. Geotherm. Resour. Counc.* 5, 221-223. 2076